Volume 45, Number 2, 2019.

Mobility & Vehicle Mechanics

International Journal for Vehicle Mechanics, Engines and Transportation Systems

ISSN 1450 - 5304

UDC 621 + 629(05)=802.0

UNIVERSITY OF KRAGUJEVAC, FACULTY OF ENGINEERING

SERBIAN SOCIETY OF AUTOMOTIVE ENGINEERS

M V M **M**obility **V**ehicle **M**echanics

*Editors: Prof. dr **Jovanka Lukić**; Prof. dr **Čedomir Duboka***

MVM *Editorial Board*
University of Kragujevac
Faculty of Engineering
Sestre Janjić 6, 34000 Kragujevac, Serbia
Tel.: +381/34/335990; Fax: + 381/34/333192

For Publisher: Prof. dr Dobrica Milovanović, dean, University of Kragujevac, Faculty of Engineering

Publishing of this Journal is financially supported from:
Ministry of Education, Science and Technological Development, Republic Serbia

Mobility & **V**ehicle **M**echanics

Motorna **V**ozila i **M**otori

Volume 45
Number 2
2019.

Mobility & **V**ehicle **M**echanics

Motorna **V**ozila i **M**otori

Volume 45
Number 2
2019.

MOBILITY & VEHICLE MECHANICS

DOI: 10.24874/mvm.2019.45.02.01
UDC: 534.321.1

A REVIEW OF FLOW ACOUSTIC EFFECTS ON A COMMERCIAL AUTOMOTIVE EXHAUST SYSTEM

Barhm Mohamad [1*]

Received in February 2019 Accepted in April 2019

RESEARCH ARTICLE

ABSTRACT: Acoustic simulation methods are being increasingly used for practical exhaust system design of automotive. In many practical applications, the sound source emits, partly, a low frequency sound spectrum comprised of superposed discrete tones and partly, a higher frequency broadband spectrum. The turbulent vortices that develop in the boundary layer between the duct wall and the flowing medium are said to generate a self-excited noise, that noise is broadband character. The self-excitation is enhanced when the flow is disturbed by irregularities in the duct wall. Unsteady compressible fluid flow through a duct is often encountered in many engineering applications and has been investigated by many researchers. When a pressure wave generated inside a duct is discharged from an open end of the duct, an impulsive wave that is usually characterized by high sound pressure level of short duration forms at the vicinity of the exit of the duct. Acoustic simulations solve the equations for motion, mass, momentum, and energy and can be divided into two methods, linear and non-linear. Through that literature review, we can analyse the methods and the latest development done on exhaust systems with regard to acoustic performance. The basic theory behind both approaches is explained as well as a source characterization technique that can be used to link the two methods. Some acoustic software tool has been applied to a variety of exhaust systems.

KEY WORDS: computational fluid dynamics (CFD), aeroacoustics, exhaust system, Helmholtz resonator, flow effect, transmission loss, muffler modeling

[1]*Barhm Mohamad, PhD student, University of Miskolc, Faculty of Mechanical Engineering and Informatics, 3515 Miskolc, Hungary, pywand@gmail.com (*Corresponding author)*

PREGLED AKUSTIČNIH EFEKATA PROTOKA NA KOMERCIJALNI AUTOMOBILSKI SISTEM

REZIME: Metode akustične simulacije se sve više koriste u praktičnom dizajnu izduvnih sistema automobila. U mnogim praktičnim primenama, izvor zvuka emituje, delimično, niskofrekventni zvučni spektar koji se sastoji od superponiranih diskretnih tonova i delimično širokopojasnog spektra veće frekvencije. Turbulentni vrtlozi koji se razvijaju u graničnom sloju između zida kanala i srednjeg toka stvaraju samo-pobuđeni šum, koji je širokopojasnog karaktera. Samo-pobuđivanje je pojačano kada je protok poremećen nepravilnostima u zidu kanala. Nestabilni protok stišljivog fluida kroz kanal se često susreće u mnogim inženjerskim primenama i istraživan je od strane mnogih istraživača. Kada se talas pritiska koji se stvara unutar kanala ispušta iz otvorenog kraja kanala, impulzivni talas koji se obično karakteriše visokim nivoom zvučnog pritiska je kratkog trajanja u blizini izlaznog kanala. Akustičke simulacije rešavaju jednačine za kretanje, masu, moment i energiju i mogu se podeliti na dve metode, linearne i nelinearne. Kroz taj pregled literature, možemo analizirati metode i najnoviji razvoj koji se radi na izduvnim sistemima s obzirom na akustične performanse. Osnovna teorija koja stoji iza oba pristupa objašnjena je kao i tehnika karakterizacije izvora koja se može koristiti za povezivanje ova dva metoda. Neki akustični softverski alati su primenjeni na različite izduvne sisteme.

KLJUČNE REČI: računska dinamika fluida (CFD), aeroakustika, izduvni sistem, Helmholtz rezonator, efekat protoka, gubitak prenošenja, modeliranje prigušivača

A REVIEW OF FLOW ACOUSTIC EFFECTS ON A COMMERCIAL AUTOMOTIVE EXHAUST SYSTEM

Barhm Mohamad

1. INTRODUCTION

Noise is therefore studied, regulated and monitored by many countries, authorities, and establishments due to the negative effects. Noise from the transportation sector, and more specifically road vehicles with internal combustion engines is something people interact within a day-to-day basis making it an important area for noise control. Manufacturers of all kinds of road vehicles strive to mitigate as much noise as possible to produce silent vehicles both due to legislation and competition.

Knowledge of the acoustic source characteristics of internal combustion engines (IC-engines) is of great importance when designing the exhaust duct system and its components to withstand the resulting dynamic loads and to reduce the exhaust noise emission. The goal of the present review is to show numerically and experimentally investigate the variety speed IC-engine acoustic source characteristics, not only in the plane wave range but also in the high frequency range define the wave equation one must first look at one – dimensional the linear conservation equation of continuity which relates density and particle velocity up in the medium. The decomposed definition of density have been inserted and higher-order terms are neglected [1].

2. MATHEMATICAL MODELS

The sound usually generated because of the coupling between the turbulent average flow field and the acoustic field is said to be self-excited. The solution to the wave equation; the general solution for free, plane and one-dimensional wave propagation:

$$P(x, t)= f(t-x/c)+g(t+x/c) \quad (1)$$

Where f and g are arbitrary functions. f(t-x/c) implies wave propagation in the positive direction along the x-axis, with the speed c and P(x, t) represent sound pressure.

We can write the linear conservation equation of continuity:

$$\frac{\partial \rho}{\partial t} + \rho o \frac{\partial u_p}{\partial x} = 0 \quad (2)$$

Where:

ρ: Acoustic density disturbance kg/m^3

ρo: Density in undisturbed medium kg/m^3

The linear in viscid conservation equations of momentum are also needed. Assuming that viscous effects can be neglected, the equation system relates velocity of the sound wave with acoustic pressure. Here, higher-order terms are also neglected.

Linear in viscid of motion:

$$\rho o \frac{\partial u_p}{\partial t} + \frac{\partial P}{\partial x} = 0 \quad (3)$$

Equation (1) and (2) include five unknown variables to solve but only four equations, similarly, as in fluid dynamics, the equation of state must be used to complete the equation system. Thermodynamic equation of state:

$$(p_o + p) = (\rho o + \rho)RT/M \quad (4)$$

Where:

Po: Pressure in undisturbed medium Pa

Pac: Acoustic pressure Pa

R: Ideal gas constant (R = 8.315) J/(mol. K)

The gas low for adiabatic changes of state:

$$\frac{(Po + P)}{Po} = \left(\frac{\rho o + \rho}{\rho o}\right)^{\gamma} \quad (5)$$

he acoustic wave equation can then be defined by subtracting the time derivative of continuity (2) from the spatial derivative of momentum (3) and eliminating ρ by inserting the equation of state (4). The governing acoustic wave equation is defined as:

Source-free linearized acoustic wave equation:

$$\frac{\partial^2 p}{\partial x^2} - \frac{1}{C^2}\frac{\partial^2 p}{\partial t^2} = 0 \quad (6)$$

The speed of sound expressed as:

$$C = \sqrt{\gamma Po/\rho o} \quad (7)$$

γ :Turbulence intermittency defining the propagation speed of an acoustic wave in the medium. The temperature dependence of the speed of sound:

$$C = Co\sqrt{T/273} \quad (8)$$

Where Co is the speed of sound at 0 °C.

There is important part in mufflers called Helmholtz Resonance chamber formed by a part of the inlet pipe and chamber is to reduce the specific frequency noise. It acting as an acoustic filter is designed to attenuate low frequency noise from engine [3]. The effects of mean flow on the acoustic properties of Helmholtz resonator and frequency domain-based Computer Aided Engineering (CAE) can describe the acoustic properties without mean flow. But to be able to design effective resonators with consideration for flow effects, a computational technique able to capture the fluid physics and acoustic behavior in the time-domain accurately is necessary. A simplified way of describing the interaction between fluid flow and acoustic wave propagation is applying the linearized Navier-Stokes equations (LNSE) [4].

$$fr = \frac{c}{2\pi}\sqrt{\frac{A_n}{V_c(L_n + \delta_n)}} \quad (9)$$

Where:

fr: Cut-off frequency

C: The speed of sound

A_n: The neck cross-sectional area

V_c: The volume of the resonator house

L_n: The length of the neck

δ_n: The end correction.

2.1 Transmission loss

There are several acoustic quantities to define the noise mitigating performance of a silencer in a duct system. The most common quantities are noise reduction (NR), insertion loss (IL) and transmission loss (TL). The NR is defined as the difference in sound pressure level (SPL) before and after the muffler. The most accepted approach today is the approach developed by authors [2] who proposed a two-source method for measuring the four-pole parameters of an acoustic element or combination of elements. The method can also be used in the presence of a mean flow.

2.2 Decomposition method

This method used for calculation transmission loss. TL with decomposition method can be expressed as:

$$TL = 10Log_{10}\frac{W_i}{W_t} \tag{10}$$

Where Wi, Wt denote incident and transmitted sound power level of the acoustic wave present in the exhaust-duct system. The equation can be written in other form to express the transmission isolation of an expansion chamber with a circular cross section and eccentrically placed inlet and outlet point:

$$D_{TL} = 10.\log(1 + (\frac{S_1}{2S_2} - \frac{S_2}{2S_1})^2 sin^2(kL)) \tag{11}$$

Where:

S_1: Cross section area of incoming of channel

S_2: Cross section area of outgoing of channel

K: Wave number

L: The length of chamber

2.2.1 Two-Source Method

The two-source method is based on the transfer matrix approach that represents the acoustic behavior of the muffler.

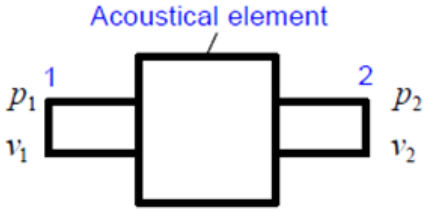

Figure 1. The four-Pole method

The transfer matrix is

$$\begin{bmatrix} P_1 \\ V_1 \end{bmatrix} = \begin{bmatrix} A & B \\ C & D \end{bmatrix} \begin{bmatrix} P_2 \\ V_2 \end{bmatrix}$$

Where P_1 and P_2 are the sound pressure amplitudes at the inlet and outlet, respectively; V_1 and V_2 are the particle velocity amplitudes at the inlet and outlet, respectively; and *A*, *B*, *C* and *D* are the four-pole parameters of the system [5].

2.2.2 Two-Load Method

The transmission loss measurement setup schematically as shows in figure 2. A speaker is placed at the end of the impedance tube. Two microphones are mounted upstream and the other two microphones are mounted downstream. Two different termination loads are applied, and four transfer functions are measured for each load [6].

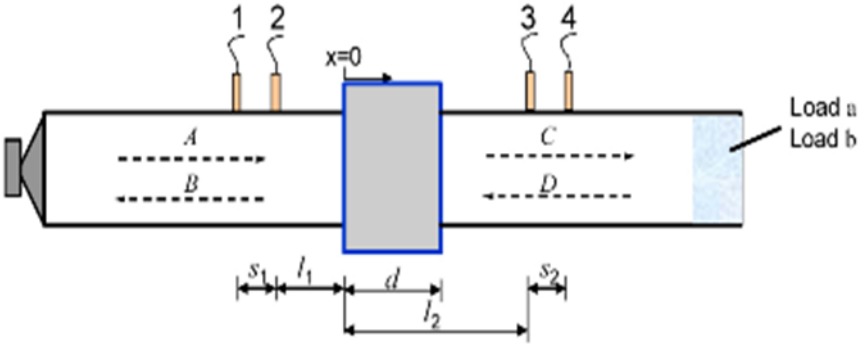

Figure 2. Two-load transmission loss test setup [6]

Tao and Seybert, studied and compared the results from two source method and two-load method calculation of transmission loss in mufflers which do not require an anechoic termination, as shows in figure 3.

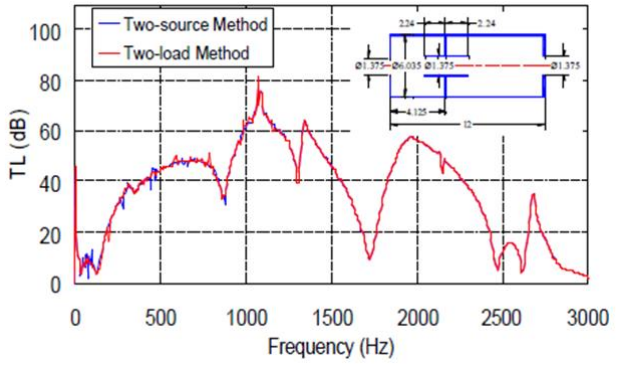

Figure 3. Validation between Two-source method and two-load method (Muffler dimensions in inches) [6]

3. SOFTWARE ANALYSIS

3.1 Software description and calculation

This chapter aims to present the numerical methods used in the further simulations to describe the mathematical models presented in literature. Only numerical methods related to CFD and how the methods are implemented in Ansys - Fluent are of interest. This means that numerical methods related to the acoustic. Authors [7] study acoustic using simulation software based on the linear and nonlinear approach and the solutions to the basic

fundamental equations for mass, momentum, and energy. The results was implied that the linear acoustic simulation can then be used to predict radiated sound and take advantage of the faster calculation times. Increasing use of after treatment devices in exhaust systems requires specific models of such components. This method is also able to utilize optimization techniques which are particularly well suited to the fast calculation speed of the linear acoustics. Authors [8] Investigate numerically and experimentally at the medium speed of internal combustion engine acoustic source characteristics and at high frequency range. One-dimensional process simulation code was used for this study. The design of exhaust system was done according to engine standard parameter.

Authors [9] discuss the transverse plane wave analysis of short elliptical end chambers, acoustical source characterization of the exhaust systems of reciprocating internal combustion engines, analysis of multiply-connected element mufflers, breakout noise of non-circular muffler shells, and analysis of porous inside the muffler.

Recently, Authors [10] have presented a two-port method for flow and pressure drop calculation as well as acoustical analysis of complex perforated-element automotive mufflers. The study proposed a new segmentation approach based on two-port analysis techniques in order to model perforated pipes using general two-port codes, which are widely available.

3.2 Flow distribution

When flow is introduced through the muffler, its transmission properties are affected in three ways. The first is through the convective effects, which affect the propagation inside straight pipes. This effect was accounted for in the formulation of the transfer matrices for different pipe elements. The second is the introduction of extra losses at the area expansion, which takes place at the end of the inlet pipe. The third and most important effect of flow is introduced by the change of the perforate impedance. The flow can be either grazing to the perforate, through the perforate, or both. The bigger effect comes from the flow through the perforate, which increases the resistance considerably.

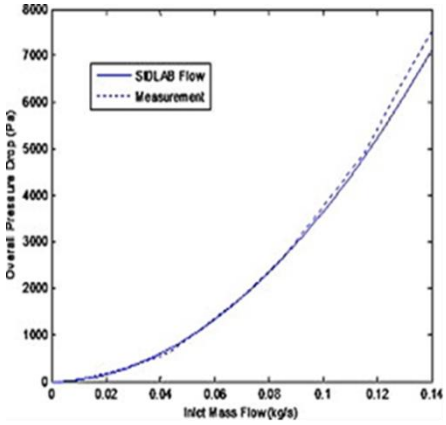

Figure 4. Pressure drop inside the prototype muffler [10]

Authors [11] considered the problem of wave propagation in short elliptical chambers having ports located along the major axis of the elliptical section. The wave propagation was considered along with the transverse direction (along with the major axis), wherein. Matrizant method was used to obtain transfer matrices relating the upstream and downstream variables. It was pointed out that such short chamber muffler characterized by

dominant transverse plane wave propagation is acoustically analogous to an extended inlet and outlet chamber. In fact, a short chamber shows a striking resemblance with a side inlet and side outlet chamber (long in the axial direction). A prerequisite for this investigation is to have realistic values of the pressure-time history. These were computed using the commercial software AVL-BOOST for different acoustical loads [12]. This finite-volume CFD model is used in conjunction with the two-load method to evaluate the source characteristics at a point in the exhaust pipe just downstream of the exhaust manifold.

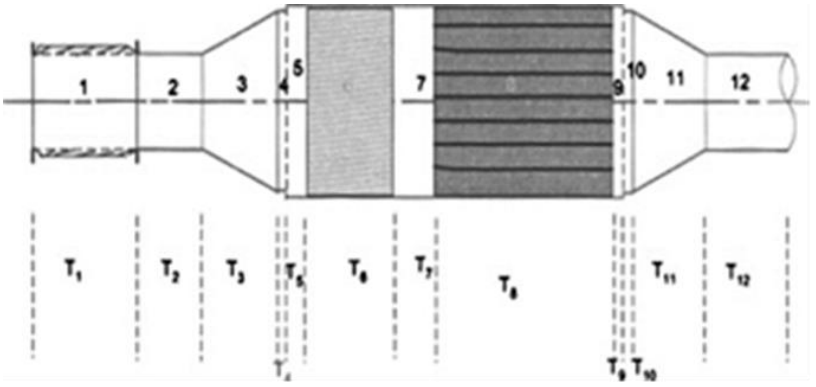

Figure 5. Sketch of the muffler internal scheme [11]

Authors [13] study muffler performance experimentally and a test rig was designed in order to measure the Transmission Loss of a set of muffler configurations in the stationary medium. The experimental set up is based in a combination of the decomposition method. It shows the geometry and comparison between the experimental and Transfer Matrix Method (TMM) modeling numerical results of TL for a high porosity perforated concentric tube inside an elliptic expansion chamber. A reasonable similarity in the transmission loss curves can be verified.

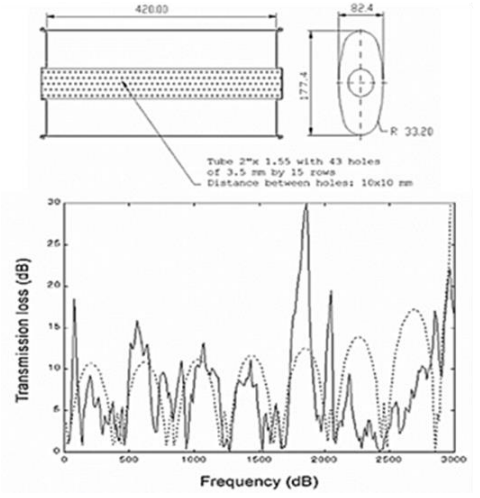

Figure 6. Transmission loss of a concentric perforate tube; TMM results and experimental result [13]

Authors [14] present a new hybrid approach or prediction of noise radiation from engine exhaust systems by making use of the time domain modeling of the cylinder and cavity pipe junction, and the linear frequency domain analysis of the muffler.

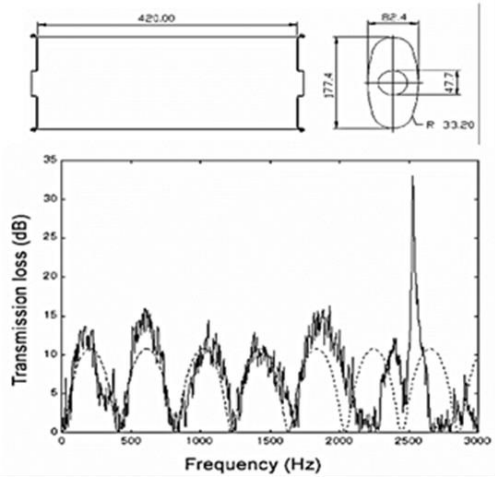

Figure 7. Transmission loss for a simple expansion chamber using an extended tube length of 0.1 mm [13]

Authors [15] had analyzed an elliptical expansion-chamber muffler as well as an end chamber muffler using a 3-D analytical method based on the modal superposition technique and the point-source method. In this figure below, the 1-D model based on the transverse plane-wave method is used to predict the transmission loss characteristics of short axial-length mufflers, taking the same dimensions as considered.

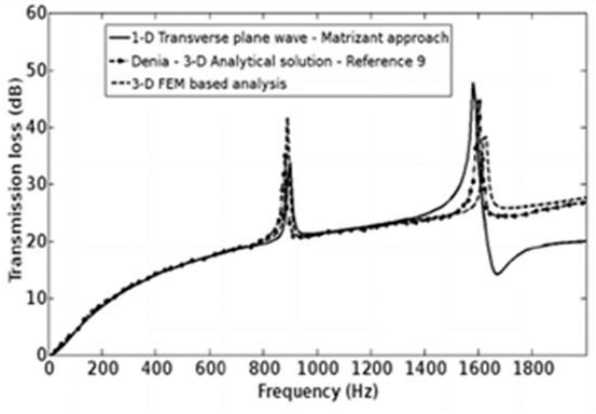

Figure 8. Acoustic performance of end-centered inlet and end-offset outlet configuration, as shown in Fig. 8a with L = 0.05 m, D 1 = 0.23 m, D 2 =0.033 m [15]

Authors [16] presented in their technical paper, the performance of circular duct with non-locally lining by numerically and experimentally. The liner concept is based on perforated screens backed by air cavities. Dimensions of the cavity are chosen to be bigger than the wavelength so acoustic waves within the liner can propagate parallel to the duct surface. The

aim of this research was to identify the best multi-cavity muffler configuration for reduction of exhaust noise from the engine. The result shows that the cavity configuration achieving the maximum overall acoustic Transmission Loss. The study also illustrates how the acoustic performances are dependent on the nature of the incident field.

Authors [17] analyzed the limitation of the net insertion loss of the muffler, by using three-pass double reversal muffler in automotive exhaust systems. This muffler is characterized by a fairly wideband transmission loss [TL] curve as well as relatively low back pressure.

Authors [18] prove experimentally, the ratio of the reduction in the back pressure at 11000 engine rpm is around 40% with open valve, as compared closed valve condition. The increase in sound transmission loss, with closed valve, is around 15∼20 dB higher when compared to open valve condition. M. Dixit et al. studied the effects of back pressure on muffler effectiveness and the simulation is carried out using GT-POWER® tool. The discretization of muffler and resonator shell and pipes for element generation had played an important role in the proper prediction of back pressure and thereby reducing valuable design cycle time and cost. Authors [19] presented in their technical paper optimization of intake exhaust system of a single-cylinder water-cooled swirl chamber diesel engine, by using computational fluid dynamics [CFD] and steady flow test method. The configurations and performances of intake and exhaust port, air filter and muffler were optimized for reducing flow resistance, increasing charge amount and lowering residual exhaust gas, leading to the improvement of engine performances and emissions, e result of this research show great achievement in engine exhaust gas properties. Authors [20] presented in their research paper the acoustic characteristics of duct muffling systems. The program was based on the plane wave theory and uses the Visual Basic 6.0 to build and modify the duct muffling systems quickly with proper the geometrical and physical parameters, to examine the effects of design changes on the acoustic attenuation characteristics and finally to get an acceptable solution.

Authors [21] was contributed to determine acoustic performance of muffler and can be reviewed for design and development of muffler. In his research paper two-load method was conducted for measuring muffler transmission loss also algorithm for computing the transmission loss was involved. It is demonstrated that the effect of adding conical adapters is significant at low frequencies especially if the adapter is short in length. It was found that measurements are improved by selecting a downstream microphone as a reference instead of an upstream microphone with good agreement for both method.

The author [22] use an acoustical topology optimization for a partition volume minimization problem achieving high value transmission loss through muffler.

Authors [23] used Computational Fluid Dynamics (CFD) methods for simulation of acoustic pulse in muffler and develop a full compressible Navier-Stokes solution algorithm for acoustic propagation problems. A new hybrid low Mach number pressure based compressible solver was developed to simulate propagation of pulses of random shape, demonstrated by application through a simple expansion muffler.

Authors [24] compared model meshing approach result with numerical analysis in various cases of length–diameter ratio to predict transmission loss of a muffler. Authors [25] studied the automotive muffler experimentally and numerically. 3D CFD was used to evaluate both mean flow and acoustic performance of an expansion chamber muffler, with various modifications including baffles an extended inlet or out let pipes.

Authors [26] studied acoustic plane wave properties of a complex geometry, and some parameter were experimentally calculated such as reflection coefficient using the TMM on the upstream and downstream side of the test object. In this research Presented and tested a method for measuring the two-port data in the form of a scattering-matrix, describing the

relationship between the traveling wave amplitudes of the pressure on either side of the test object.

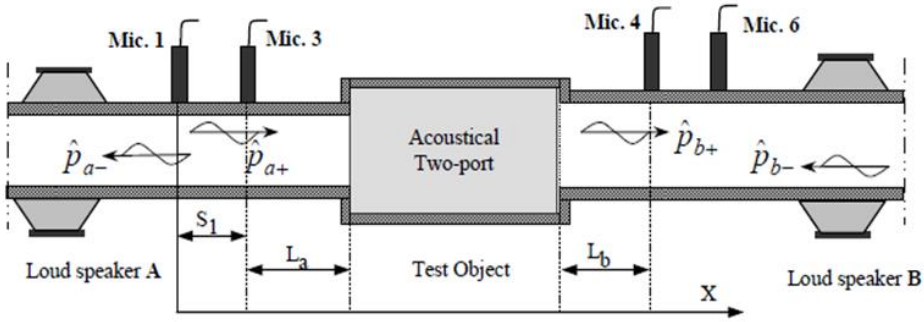

Figure 9. Acoustical Two-Part method for a muffler [26]

Linear and passive two-port in the frequency domain, be written:

$$X=TY \tag{12}$$

Where, X/Y are the state vectors at the input/output and T is a [2×2]-matrix, which is independent of Y. To determine T, from measurements four unknown must be determined.

The transfer-matrix form uses the acoustic pressure P and the volume velocity V.
$X = [P_a, V_a]$ and $Y = [P_b, V_b]$ here [a] and [b] represent two different ducts cross section. The transfer-matrix could be written in the following form:

$$\begin{bmatrix} P_a \\ V_a \end{bmatrix} = \begin{bmatrix} T_{aa} & T_{ab} \\ T_{ba} & T_{bb} \end{bmatrix} \begin{bmatrix} P_b \\ V_b \end{bmatrix} \tag{13}$$

$$Pa = P+\exp(-ikaLa)+P-\exp(ikaLa) \tag{14}$$

$$V_a = \frac{A_a}{\rho c}\{(P_+\exp(-ik^aL_a)-P_-\exp(ik^aL_a)\}$$

and

$$\begin{aligned} P_b &= P_+\exp(-ik^bL_b)+P_-\exp(ik^bL_b) \\ V_b &= \frac{A_b}{\rho c}\{(P_+\exp(-ik^bL_b)-P_-\exp(ik^bL_b)\} \end{aligned} \tag{15}$$

The result shows, the acoustic two port, of a single diaphragm orifice and then validated with the theoretical result has been calculated using 3D FEM software FEMLAB from other literatures.

The author [27] present different approaches for measurement and evaluation of the source characteristics of an engine exhaust system have been briefly reviewed, with particular emphasis on their relative implications and limitations. These approaches combine the advantages of the frequency-domain analysis of mufflers with those of the time-domain analysis of the exhaust manifold source. Because in some method does not require prior knowledge of the source characteristics, like piston motion, exhaust valve/port opening and high blow-down pressure in the cylinder.

4. CONCLUSIONS

The main contribution of the present review, as well as the development of an expression for the non-dimensional frequency for obtaining the resonance peak in the TL graph for the short chambers with end ports, is another noteworthy contribution of this present review. This enables a muffler designer to have a quick estimate of the positions of the peak and trough in the TL spectra for short chamber mufflers and to get a qualitative understanding of the basic nature of such short chamber mufflers.

REFERENCES

[1] Linus Zackrisson. Flow Acoustic Effects on a Commercial Automotive Air Intake Silencer A Numerical Study using Computational Fluid Dynamics. *Journal of Applied Mechanics*. Chalmers University of Technology, 2017.

[2] M. L. Munjal, and A. G. Doige. Theory of a Two Source-location Method for Direct Experimental Evaluation of the Four-pole Parameters of an Aeroacoustic Element. *Journal of Sound and Vibration*, Vol.141, No. 2, 1990, pp 323-333.

[3] Takashi Yasuda, Chaoqun Wu, Noritoshi Nakagawa and Kazuteru Nagamura. Studies on an automobile muffler with the acoustic characteristic of low-pass filter and Helmholtz resonator. *Applied Acoustics,* Volume 74, Issue 1, 2013.

[4] Hans Bodén, Ulf Carlsson, Ragnar Glav, Hans-Peter Wallin, and Mats Åbom. *Sound and vibration*. The Marcus Wallenberg Laboratory, KTH, 2003.

[5] Z. Tao and A. F. Seybert. A Review of Current Techniques for Measuring Muffler Transmission Loss. *Society of Automotive Engineers*, Inc.1653-01-2003.

[6] X. Hua and D. W. Herrin. Practical Considerations when using the Two-Load Method to Determine the Transmission Loss of Mufflers and Silencers. *SAE International*, 2013.

[7] R. Glav, M. Abom and R. Fairbrother. Acoustic modeling for practical intake and exhaust system design. *4th International styrian noise, vibration and harshness congress*, 2006.

[8] A. Hynninen, R. Turunen, M. Åbom, and H. Bodén. Acoustic Source Data for Medium Speed IC-Engines. ASME. *J. Vib. Acoust*. doi:10.1115/1.4006415, 2012.

[9] M. L. Munjal. Recent Advances in Muffler Acoustics. *International Journal of Acoustics and Vibration*, Vol. 18, No. 2, 2013.

[10] T. Elnady, M. Abom and S. Allam. Modeling perforates in mufflers using two-ports, *ASME Journal of Vibration and Acoustics*, 132, 2010, pp 1–11.

[11] A. Mimani and M. L Munjal. Transverse plane wave analysis of short elliptical chamber mufflers — An analytical approach, *Journal of Sound and Vibration*, 330, 2011, pp 1472–1489.

[12] BOOST Version 5.0.2, AVL LIST GmbH, Graz, Austria, 2007.

[13] Y. Gerges, R. Jordan, A. Thieme, L. Coelho and P. Arenas. Muffler modeling by transfer matrix method and experimental verification. Journal of the Brazilian. *Society of Mechanical Sciences and Engineering*, Vol. 27, No. 2, 2005, pp 132-140.

[14] Y Sathyanarayana and M. L. Munjal. Hybrid approach for aeroacoustic analysis of the engine exhaust system. *Applied Acoustics*. 60, 2000, pp 425-450.

[15] F. D. Denia, Albelda, F. J.Fuenmayor and A. J. Torregrosa. Acoustic behaviour of elliptical chamber mufflers, *Journal of Sound and Vibration*, Vol. 241, No. 3, 2001, pp 401–421.

[16] B. Ouédraogo, R. Maréchal, J.-M. Ville, and E. Perrey-Debain. Broadband noise reduction by circular multi-cavity mufflers operating in multimodal propagation conditions. *Applied Acoustics*, 107, 2016, pp 19-26.

[17] V. Sagar, M. L. Munjal. Design and analysis of a novel muffler for wide-band transmission loss, low back pressure and reduced flow-induced noise. *Noise Control Engineering Journal* Vol. 64, No. 2, 2016, pp 208-216.

[18] S. Talegaonkar, M. R. B. Agrewale, and K. Vora Chhaganlal. Design and Development of Tunable Exhaust Muffler for Race Car. *SAE Technical Papers International Mobility Conference*, SIIMC 2016.

[19] S.J, Liu, J. J Zeng, W.W. Han, Y. Chen, and J. Wang. Intake and exhaust system performance of diesel engine based on CFD and steady flow test method Neiranji Xuebao/Transactions of CSICE [*Chinese Society for Internal Combustion Engines*] Vol. 34, No. 1, 2016, pp 68-73.

[20] Ji. Zhenlin and Fan Yiliang. MAP: a Simulative Program for Acoustic Prediction and Analysis of Duct Muffling Systems. DOI: 10.4271/2015-01-2317, 2015.

[21] X. Hua, Y. Zhang, and D.W. Herrin. The effect of conical adapters and choice of reference microphone when using the two load method measuring muffler transmission loss. *Applied Acoustics*, Vol. 93, No. 6, 2015, pp 75-87.

[22] Jin Woo Lee. Optimal topology of reactive muffler achieving target transmission loss values: Design and experiment. *Applied Acoustics*, Vol. 88, No. 2, 2015, pp 104-13.

[23] Nishant K. Singh, and Philip A. Rubini. Large Eddy Simulation of acoustic pulse propagation and turbulent flow interaction in expansion mufflers. *Applied Acoustics*, Vol. 98, No. 11, 2015, pp 6-19.

[24] C.J. Wu, X.J. Wang, and H.B. Tang. Transmission loss prediction on a single-inlet/double-outlet cylindrical expansion chamber muffler by using the modal meshing approach. *Applied Acoustics*, Vol. 69, No. 2, 2008, pp 173-178.

[25] Takashi Yasuda, Chaoqun Wu, Noritoshi Nakagawa, and Kazuteru Nagamura. Predictions and experimental studies of the tail pipe noise of an automotive muffler using a one-dimensional CFD model. *Applied Acoustics*, Vol. 71, No. 8, 2010, pp 701-707.

[26] S. Allam, H. Bodén & M. Åbom. Over-Determination in Acoustic Two-Port Data Measurement. *The Thirteenth International Congress on Sound and Vibration*. Vienna-Austria, 2006.

[27] M. L. Munjal. Acoustic Characterization of an Engine Exhaust Source – A Review. *Proceedings of Acoustics*, 2004.

Intentionally blank

MOBILITY & VEHICLE MECHANICS

DOI: 10.24874/mvm.2019.45.02.02
UDC: 621.822

ANALYSIS OF THE INFLUENCE OF INTERNAL RADIAL CLEARANCE ON THE LOAD DISTRIBUTION OF THE ROLLING BALL BEARING

Sonja Kostić [1], Zorica Đorđević [2], Milosav Đorđević [3], Saša Jovanović [4]*

Received in December 2018 Revised in March 2019 Accepted in April 2019

RESEARCH ARTICLE

ABSTRACT: The distribution of the external radial load on rolling bodies of bearing is uneven. This is a statically undefined problem, so for the analysis of load distribution beside equilibrium conditions need to be introduced and supplemental one which are based on the relationship between the contact deformation of the contact parts and loads. The unevenness of the distribution is greater considering the influence of the inner radial clearance. Purpose of the paper is to determine the load transmitted by the most heavily loaded rolling body as well as the other rolling bodies, used analytical and numerical approach.

KEY WORDS: radial ball bearing, internal radial clearance, load distribution, Finite Element Method

[1]*Sonja Kostić, MSc, University of Kragujevac, High Technical School of Vocational Studies in Kragujevac, Kosovska 8, 34000 Kragujevac, sonja25yu@yahoo.com (*Corresponding author)*
[2]*Zorica Đorđević, PhD assoc. prof., University of Kragujevac, Faculty of Engineering Kragujevac, Sestre Janjic 6,34000 Kragujevac, zoricadj@kg.ac.rs*
[3]*Milosav Đorđević, PhD prof., University of Kragujevac, High Technical School of Vocational Studies in Kragujevac, Kosovska 8, 34000 Kragujevac, m.djordjevic.kg@gmail.com*
[4]*Saša Jovanović, Assist. prof., University of Kragujevac, Faculty of Engineering Kragujevac, Sestre Janjic 6,34000 Kragujevac, dviks@kg.ac.rs*

ANALIZA UTICAJA UNUTRAŠNJEG RADIJALNOG ZAZORA NA RASPODELU OPTEREĆENJA KOD RADIJALNOG KUGLIČNOG LEŽAJA

REZIME: Raspodela spoljašnjeg radijalnog opterećenja na kotrljajna tela ležaja je neravnomerna. To je statički nedefinisan problem, pa je za analizu raspodele opterećenja pored ravnotežnih uslova potrebno uvesti i dopunske koje se temelje na odnosu između kontaktne deformacije kontaktnih delova i opterećenja. Nejednakost raspodjele je veća s obzirom na uticaj unutrašnjeg radijalnog zazora. Cilj rada je da se odredi opterećenje koje prenosi najteže opterećeno telo valjaka kao i druga tela valjanja, koristeći analitički i numerički pristup.

KLJUČNE REČI: radijalni kuglični ležaj, unutrašnji radijalni zazor, raspodela opterećenja, metoda konačnih elemenata

ANALYSIS OF THE INFLUENCE OF INTERNAL RADIAL CLEARANCE ON THE LOAD DISTRIBUTION OF THE ROLLING BALL BEARING

Sonja Kostić, Zorica Đorđević, Milosav Đorđević, Saša Jovanović

1. INTRODUCTION

The distribution of the external radial load to the roller bodies of the radial ball bearing is uneven which means that at the same time all balls are not equal in the transfer of loads from one ring to the other. The total external load is transmitted from one ring to the other only through a certain number of total balls. The unevenness of the distribution of the external load is influenced by the intensity of the load, the inner radial clearance, the elastic deformation of the bearing rings, the internal bearing geometry and other factors. In this paper, a detailed analysis of the influence of the inner radial bearing clearance on the distribution of the external load on the roller bearing bodies is given.

2. DETERMINATION OF EXTERNAL LOAD DISTRIBUTION TO THE BALL BEARING ROLLING ELEMENTS

It is a statically undefined problem, therefore, for static equilibrium analysis it is necessary to introduce additional ones which are based on the connection between the contact deformations of the connected parts of bearing (moving one ring in relation to the other under the influence of the external load) and the load.

Consideration of the load distribution on the ball bearing rolling elements is carried out assuming that the bearing parts are stationary; that all balls of the exact dimensions and shapes and that the diameters and radii of the rolling path of the rings are of perfectly accurate measures, shape and position.

2. 1 Radial ball bearing with internal radial clearance

An analysis of the distribution of the external load to the ball bearing rolling elements will take into account that the housing in which the outer bearing ring is fitted is hard (does not change the shape due to the load) and that the direction of the external load action passes through the center of one of the ball and is directed to the ball. The external radial force F_r is distributed unevenly to a number of balls z_s in a loaded zone below the meridian plane which represents the plane of the bearing normal to the direction of the attack line of force (Figure 1). The Meridian plane divides the bearing into two zones - one is placed unloaded and in the other there are loaded balls. Balls whose centers lie at the meridian level do not transmit the load.

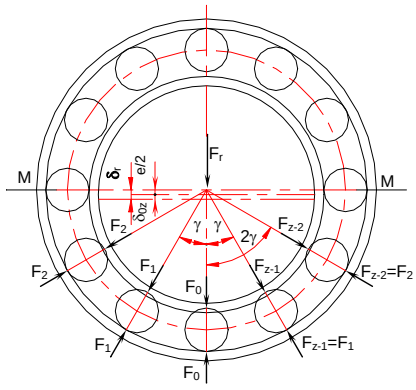

Figure 1. Load distribution to ball bearing rolling elements of radial bearings with internal radial clearance

From the static equilibrium conditions, the relationship between the external radial load and the force at the place of the most loaded ball and the force at the place of other balls can be determined. As this is a statically indeterminate/undefined problem,additional conditions are introduced which connect elastic contact deformations and loads [1], [2], [3]. It is assumed that in the unloaded state at the centric position of the rings the touching of the balls and the outer ring is achieved and that there is a radial clearance which is equal to half of the total clearance between the balls and the inner ring, as shown in Figure 1.

The distribution of the external load on the ball bearing rolling elements of radial bearings with radial clearance is radically uneven compared to the bearing without radial clearance, as the clearance increases with the increase in the load area and increases the intensity of the force at the point of the most loaded ball. Therefore, the total contact deformation at the place of the most loaded ball δ_{0z} at the initial touch point is higher than the corresponding contact deformation of the bearing without a radial clearance δ_0.

The total contact deformation of the coupled parts at the initial point of contact at the place of the most loaded ball in the existence of the radial clearance δ_{0z} is determined by iterative method using the Newton's iteration method (tangent method) [2], where by determining an unknown parameter δ_x we obtain:

$$\delta_{0z} = \frac{e}{2} \cdot \delta_x \tag{1}$$

When δ_{0z} is determined, the total radial displacement of the bearing axis δ_r can be determined, and on the basis of this the total contact deformation at the position of the random i-th ball δ_{iz} can be determined. Depending on the calculated values of the total contact deformations δ_{0z} and δ_{iz}, the corresponding forces can also be determined at the place of the most loaded ball bearing with a radial clearance:

$$F_{0z} = C_\delta \cdot \delta_{0z}^{3/2} \tag{2}$$

and at the place of random i-th balls:

$$F_{iz} = C_\delta \cdot \delta_{iz}^{3/2} \tag{3}$$

By knowing the total contact deformation of the coupled parts at the place of the most loaded ball of bearing with a radial clearance, the factor of unevenness of load distribution on the balls of the given bearing can finally be determined:

$$k = \frac{F_{0z}}{\left(\frac{F_r}{z}\right)} = \frac{C_\delta \cdot \delta_{0z}^{3/2}}{\left(\frac{F_r}{z}\right)} \tag{4}$$

From the above expression, it can be seen that the factor of unevenness of load distribution on the balls of a given bearing depends on the size of the external radial load Fr, the number of balls z, the inner bearing geometry and the elastic modulus and the Poisson coefficients of the bearing parts (constant C_δ) and the total contact deformation of the coupled parts at the starting point of the contact δ_{0z}. For a particular bearing and at a given external load, the factor *k* is only in function of δ_{0z}. Since δ_{0z} depends on the external load and the internal radial clearance e, for the given external load factor *k* is the function of the inner radial clearance. As the higher values of the radial clearance increase the contact deformation of the coupled parts, the greater is the unbalanced load distribution factor of the balls of the given bearing *k*.

2.2 An analytical example of the determination of the external load distribution on the ball bearing rolling elements

Determination of external radial load distribution parameters on the ball bearing rolling elements is performed on a single ball bearing with radial contact 6206. This bearing has a wide application in industry. In the automotive industry, it is an inevitable part of the componentes in transmission system (gearboxes, differentials...), waterpump systems, alternators, wheels etc at commercial and special vehicles. The bearing characteristics required for calculation are given in the literature [3].

For different values of the radial clearance e whose value ranged from 0 to 20 μm and for different values of the external radial load whose values ranged from 1000 to 9000 N, there is obtained table of the results of the calculation (Table 1).

Table 1. Results of the calculation for ball bearing 6206

e	Results of the calculation		F_r, N				
μm			1000	3000	5000	7000	9000
0	F_0	N	487.2	1461.7	2436.2	3410.7	4385.2
	F_{1-8}		326.6	980.0	1633.4	2286.7	2940.1
	F_{2-7}		35.2	105.7	176.2	246.80	317.3
10	F_0	N	537.6	1543.8	2534.8	3522.2	4507.2
	F_{1-8}		301.7	950.3	1599.2	2249.3	2899.9
	F_{2-7}		-	5.7	43.0	90.8	143.3
20	F_0	N	581.8	1607.8	2618.1	3622.7	4620.1
	F_{1-8}		272.9	908.6	1554.6	2204.3	2853.4
	F_{2-7}		-	-	-	0.962	23.4

Based on the obtained results, the load distribution dependency on the rolling balls depends on the intensity of the external load (Figure 2 - Figure 3) in the function of the radial clearance.

By analysing the obtained results and the diagrams presented it is concluded that increasing the intensity of the external radial load linearly increases the load values transmitted by the rolling elements of the bearing. It can be seen that increasing radial clearance increases the value of force on the site of the most loaded balls and reduces the loads of other balls involved in the distribution. This increases the unbalance of the load distribution on the rolling elements as the overall contact deformation increases on the site of the most loaded balls and reduces the contact deformations of the joined parts at the spots of the other balls. For the sake of clarity, on the diagrams, a dashed line represents the load value that the rolling elements transpose when ball bearing has no clearance.

Theoretically, in the case of large internal radial clearance in the bearing and at certain external loads, the load distribution on the ball bearing rolling elements is very unfavorable, regarding the expected balls do not come in contact, so that a large part of the external load is transmitted by the ball at line of attack force. Only after the great contact deformation of the coupled parts comes the contact of the other rolling elements.

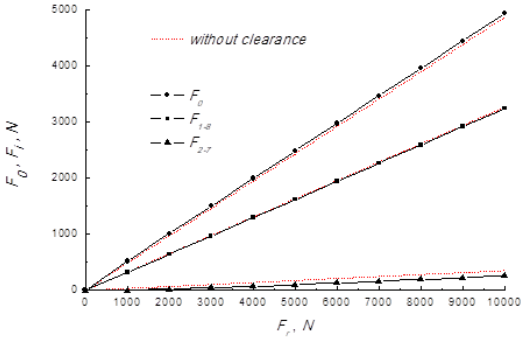

Figure 2. Load distribution on ball bearing rolling elements of 6206 depending on external load, in case of bearing with internal radial clearance (e=10 μm)

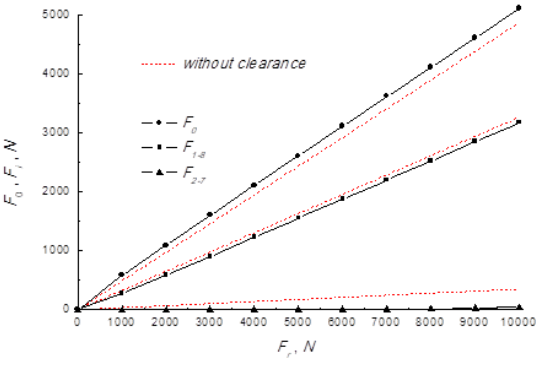

Figure 3. Load distribution on ball bearing rolling elements of 6206 depending on external load, in case of bearing with internal radial clearance (e=20 μm)

Table 2 gives the results of factor of uneven load distribution in the function of radial clearance *e*.

Table 2. Factor of uneven load distribution for ball bearing 6206

e	Results	F_r, N				
μm		1000	3000	5000	7000	9000
0	k	4.385	4.385	4.385	4.385	4.385
10		4.838	4.631	4.562	4.528	4.507
20		5.236	4.823	4.712	4.657	4.620
30		5.632	5.015	4.849	4.767	4.716

Based on the presented solutions, diagrams of factor changes of balls uneven load distribution in function of the inner radial clearances are given (Figure 4). The figure shows that the values of the factor k = 5 correspond to the radial clearance $e \approx 29\mu m$ (at a given external load, eg F = 3000 N), and that for other values of the clearance it changes (bigger or smaller). It is concluded that for the different clearances values the same value of factor of uneven the load distribution on balls k = 5, as it appears in the literature [4], can't be taken but the actual value (calculated values given in the table). This is especially important when designing bearings and supporting elements in general when the analysis of load distribution plays an important role. Taking into account the actual value of factor k it is possible to determine more precisely the static bearing load. For the sake of visibility the curvature depends only on the external load in the interval $F_r = 1000 \div 5000N$.

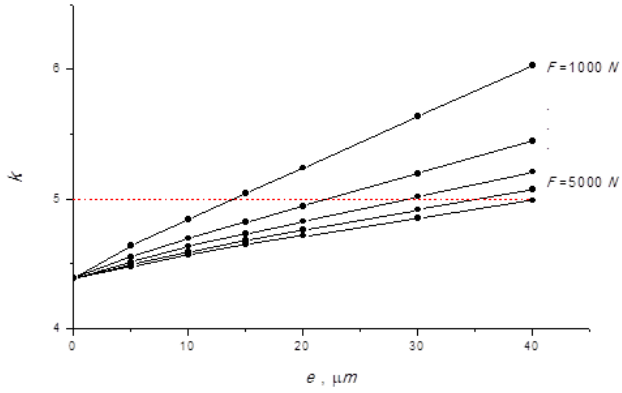

Figure 4. Change of factor of uneven load distribution to the ball bearing rolling elements in function of the radial clearance, and for the given external load

3. THE CHOICE AND MODELLING OF SIMPLIFIED REAL AND FEM MODELS OF SINGLE ROW DEEP GROOVE RADIAL BALL BEARING FOR ANALYSIS OF LOAD DISTRIBUTION OF BALL BEARING ROLLING ELEMENTS

In Figure 5, a 2D plane mesh model of finite elements for single row radial ball bearing 6206, which has nine balls, is given (the worst moment is shown when one of the balls is on the attack line of the given external load). For the discretization of the 2D physical model, 2D four-node isoparametric finite elements were used. During generalization of 2D mesh of finite elements a plane state is chosen (it is assumed that in all cross-sections of bearing the stress distribution is the same) as well as very precise division of finite elements mesh.

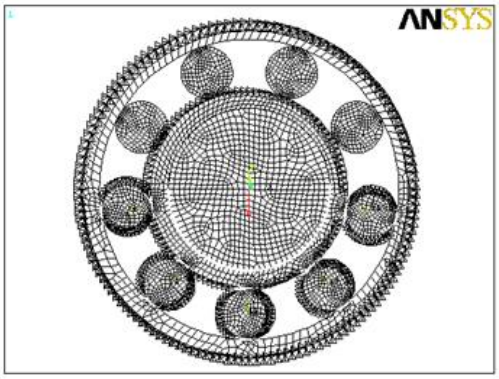

Figure 5. The mesh of 2D finite elements for the model of radial bearing 6206 with defined contact finite elements, boundary conditions (twisted coordinate system) and external load

Model of the bearing is presented in x-y global Descartes' coordinate system with its ground zero in axis of inner bearing ring. Balls bearing have local coordinate systems. Ball that is in the line of offensive force (line of y-axis) has the same coordinate system as global model bearing system with its ground zero in the centre of the ball. Other balls have twisted coordinate systems compared to the global one with its ground zero placed in the center of them. For the sake of simplified simulation of load and data observing the model is set in such a way that external load is given in the line of y-axis (radial direction). Thus the total contact deformation of the most stressed ball (the relative displacement of bearing) could be seen from results obtained from FEM analysis as node displacement in the direction of y-axis of global coordinate system. Outer bearing ring is absolutely immobilized (boundary conditions are given so that displacement is not allowed neither in line of x-axis nor y-axis). Inner bearing ring is limited in line of x-axis that is its displacement is allowed in the line of external load. The ball placed in the line of external load has exactly the same boundary conditions as inner bearing ring. The limitations of the balls in the line of external offensive line are given in radial twisted coordinate systems. Boundary conditions are given so that imitate the cage where balls are placed in the real environment. The displacement is allowed in the radial direction (direction that connects the center of model bearing to appropriate balls center). In the perpendicular direction in the radial axis of twisted coordinate system, the displacement equals zero. Without boundary conditions defined that way balls were simply sliding along model during experiment (by giving them the external load). Nodes placed in expected contact zone of balls with outer and inner bearing ring have no boundary

conditions. External radial load is given in the ground zero of global coordinate system of bearing model and variates from 1000 up to 5000 N.

The results error obtained by FEM is less than 10% compared to theoretic results.

From figure 6, the distribution of the given external radial load to the ball bearing rolling elements for the case of ball bearing without internal radial clearance is clearly visible. The most loaded ball in the bearing is ball in the direction of the action of the external load then the balls left and right of the most loaded ball. Balls right below the meridian plane are the least involved in the distribution of loads. It should be emphasized that the load values distribution by the corresponding balls left and right from the most loaded are equal which is another indication of the validity of the adopted numerical bearing model.

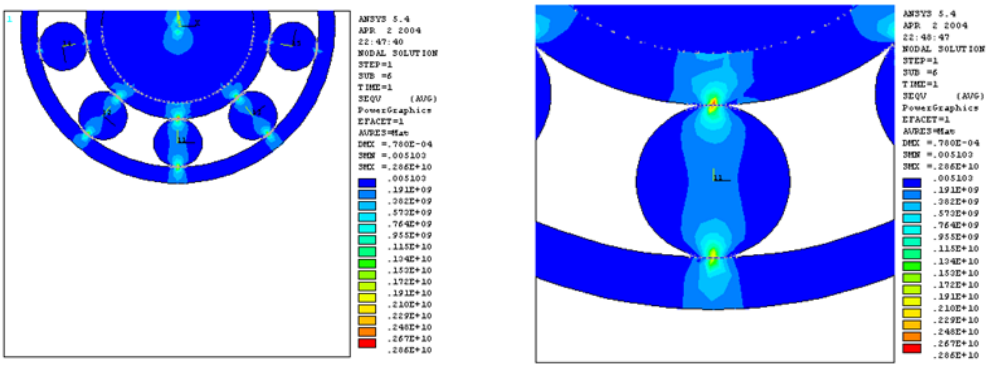

Figure 6. Numerical results of load distribution on ball bearing 6206 under the external radial load for the case of ball bearing without internal radial clearance

In Figure 7 and 8, the influence of the inner radial clearance on the load distribution is obvious. As obtained from the analytical calculation and numerical models results have been confirmed that balls located just below the meridian plane (and farthest from the most loaded ball for the given external loads) do not come into contact until a large contact deformation occurs.

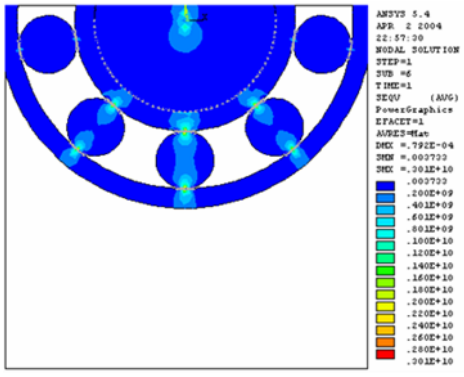

Figure 7. Numerical results of load distribution on ball bearing 6206 under the external radial load for the case of ball bearing with internal radial clearance

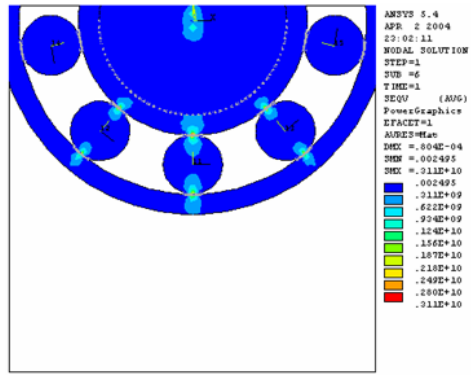

Figure 8. Numerical results of load distribution on ball bearing 6206 under the external radial load for the case of ball bearing with internal radial clearance

$e \approx 10\mu m$ $e \approx 20\mu m$

For the additional verification of the accuracy of numerical solutions, a case in the literature was provided, bearing 6306, the results of which were compared with the available theoretical [4] and numerical [5] solutions. The appearance of the 2D model of the finite elements of the radial ball bearing 6306 and the boundary conditions are identical to the bearing 6206 whose words are already detailed. Figure 9 clearly shows that results obtained by using FEM described above are more than satisfactory. Results error of FEM analysis compared to theoretic data is less than 1% (note: results are obtained by giving the external load on 6306 bearing). Comparison of the results obtained by both, ANSYS and I-DEAS Supertab softwares, demonstrate that numeric results of ANSYS are more precise to theoretic data [4] than that of I-DEAS Supertab [5].

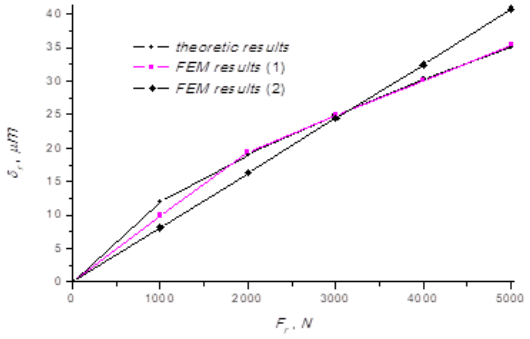

Figure 9. Graphic demonstration of the results comparison (total radial axis displacement of 6306 bearing and intensity of external load are compared) according: Theoretic research, FEM analysis by using of I-DEAS Supertab software -curve (2), [5] and FEM analysis by using of ANSYS software - curve (1)

4. CONCLUSIONS

Due to the complexity of the problem the numeric model of the ball bearing mentioned above is developed. The Finite Element Method is the numerical method used. Software used is ANSYS v.5.4. The choice and modelling of single row radial ball bearing for load distribution on ball bearing elements and stress deformation state analysis is detailed in literature. Obtained results confirmed the theoretic approach to the problem of load distribution on ball bearing elements analysis (the error of obtained results compared to the theoretic ones did not excess 10%). The same approach of ball bearing modelling could be applied to other series and ball bearing types as well. The future exploration of this problem will be directed to 3D modelling and obtaining the most reliable results possible.

ACKNOWLEDGMENT

This paper presents the results obtained during research within the framework of the projects TR 33015, supported by the Ministry of Education, Science and Technological Development of the Republic of Serbia.

REFERENCES

[1] Harris T.A., "Rolling Bearing Analysis", New York, 1984.

[1] Ristivijevic M., Mitrović R.: "Load distribution – tooth gearing and rolling bearings", Faculty of Mechanical Engineering, Belgrade, 2002.

[2] Kostić (Stefanović) S., "Analysis of the Influence of Elastic Deformation and Internal Radial Clearance on the Static Load Rating of the Rolling Ball Bearing", Master thesis, Kragujevac, 2004.

[3] Mitrović R., "Influence of Elastic Deformation and Internal Radial Clearance Analysis on the External Load Distribution of the Ball Bearing Rolling Elements", Master thesis, Belgrade, 1987.

[4] Subic, A., "Geometry Modelling of Ball Bearing with Numeric Displacement Definition in Bearing Arrangement", Master thesis, Belgrade, 1991.

Intentionally blank

MOBILITY & VEHICLE MECHANICS

DOI: 10.24874/mvm.2019.45.02.03
UDC: 621.43

A PRELIMINARY ASSESSMENT OF RESIDENTIAL APPLICATION OF INTERNAL COMBUSTION ENGINE BASED COGENERATION IN SERBIAN CLIMATIC CONDITIONS WITH BUILDING SIMULATION PROGRAM

Novak Nikolić [1], Nebojša Lukić [2], Nikola Milutinović [3], Aleksandar Nešović [4]*

Received in February 2019 Accepted in April 2019

RESEARCH ARTICLE

ABSTRACT: In this paper the energetic and economic performance assessment of residential application of IC engine based cogeneration system in the Serbian climatic conditions using building energy simulation software was performed. The performance of IC based system was compared with the performance of the two other conventional systems for DHW preparation: gas and electric water heater. Comparing the IC based system with gas water heater the period required to return investment costs of IC engine is relatively high (11.7 years). The main barriers for widespread residential application of IC engine cogeneration system are related to the high capital costs and low price of purchased or sold electricity. In this respect, the investment cost reduction in small scale cogeneration systems has to be achieved. In relation to the current price in Serbia the price of purchased and sold electricity (feed-in tariff) should be increased by 37.5% and 67.5%, respectively, in order to achieve the value of payback period of five years.

Comparing the IC based system with electric water heater the application of the IC engine is economically feasible since the payback period amounts 3.42 years. According to the simulation results, the IC engine cogeneration system ensured a primary energy saving of 28.81%.

KEY WORDS: cogeneration, internal combustion engine, primary energy saving, dynamic simulation

[1]*Novak Nikolić, PhD Assist. professor, University of Kragujevac, Faculty of Engineering, Sestre Janjić 6, 34000 Kragujevac, novak.nikolic@kg.ac.rs (*Corresponding author)*
[2]*Nebojša Lukić, PhD prof., University of Kragujevac, Faculty of Engineering, Sestre Janjić 6, 34000 Kragujevac, lukic@kg.ac.rs*
[3]*Nikola Milutinović, MSc Student, University of Kragujevac, Faculty of Engineering, Sestre Janjić 6, 34000 Kragujevac, nikola.milutinovic95@gmail.com*
[4] *Aleksandar Nešović, PhD Student, University of Kragujevac, Faculty of Engineering, Sestre Janjić 6, 34000 Kragujevac, aca.nesovic@gmail.com*

PRELIMINARNA PROCENA PRIMENE KOGENERACIJE NA BAZI MOTORA SA UNUTRAŠNJIM SAGOREVANJEM U STAMBENOM SEKTORU U KLIMATSKIM USLOVIMA SRBIJE UZ POMOĆ PROGRAMA ZA SIMULACIJU PONAŠANJA ZGRADA

REZIME: U ovom radu izvršena je procena energetskih i ekonomskih performansi primene kogenerativnog sistema na bazi motora SUS u stambenom sektoru u srpskim klimatskim uslovima korišćenjem softvera za simulaciju energetskog ponašanja zgrada. Performanse sistema baziranog na SUS motoru su upoređene sa performansama druga dva konvencionalna sistema za pripremu PTV: gasnim i električnim zagrejačem vode. Upoređujući SUS motor sa gasnim zagrejačem, period potreban za povraćaj investicionih troškova motora relativno je visok (11,7 godina). Glavne prepreke za širu primenu kogenerativnog sistema SUS motora odnose se na visoke kapitalne troškove motora SUS i nisku cenu otkupljene ili prodate električne energije. U tom pogledu, neophodno je postići smanjenje investicionih troškova kogenerativnih sistema malih snaga. U odnosu na trenutnu vrednost u Srbiji, vrednost cene otkupljene i prodate električne energije (feed-in tarife) treba da se poveća za 37,5% odnosno 67,5%, respektivno, kako bi se dostigla vrednost perioda otplate od pet godina. Upoređujući sistem baziran na SUS motoru sa električnim zagrejačem vode, primena SUS motora ekonomski je isplativa obzirom da period povraćaja investicije iznosi 3,42 godine. Prema rezultatima simulacije, kogenerativni sistem SUS motora obezbeđuje uštedu primarne energije od 28,81%.

KLJUČNE REČI: kogeneracija, motor sa unutrašnjim sagorevanjem, primarna ušteda energije, dinamička simulacija

A PRELIMINARY ASSESSMENT OF RESIDENTIAL APPLICATION OF INTERNAL COMBUSTION ENGINE BASED COGENERATION IN SERBIAN CLIMATIC CONDITIONS WITH BUILDING SIMULATION PROGRAM

Novak Nikolić, Nebojša Lukić, Nikola Milutinović, Aleksandar Nešović

1. INTRODUCTION

Cogeneration (CHP) represents the process of simultaneous or combined production of electrical (or mechanical) and thermal energy using a single primary energy source (fuel) within an integrated system. The main reasons for the application of the concept of cogeneration are reflected in the significantly higher efficiency of transformation and use of primary energy. In other words, cogeneration plants, in relation to separate electricity and thermal generation plants, contribute to higher primary energy savings, higher economic savings and reduction of greenhouse gas (GHG) emissions. The main components of the CHP plants are prime mover (heat engine), generator and heat recovery (heat exchanger). The CHP plants are categorized according to the type of prime mover which can be as: internal combustion engine (IC engine); gas turbine; steam turbine and fuel cell. The IC engine as the main part of the cogeneration system provides mechanical energy which is transformed into electrical energy as well as thermal energy by recovering heat from hot exhaust gases, water cooling system and lube oil system. Reciprocating IC engines used for residential cogeneration applications of less than 30 kW are frequently based on spark ignition engines that are mostly run on natural gas [1]. In relation to the other prime movers, the IC engines offer easy and fast start up, significant low and medium temperature heat recovery and occupy a small area in relation to the installed capacity.

Small scale residential cogeneration systems have been studied by many researchers on experimental and simulation basis. Aussant et al. [2] modelled and simulated two IC engine cogeneration units (1 kW_{el} and 2 kW_{el}) providing thermal and electric energy to a Canadian residential houses. The results have shown that the CHP efficiency of the 1 kW_{el} system was found to be higher than the 2 kW_{el} system. They have found a net reduction of GHG emissions of approximately 20%. Gonçalves et al. [3] experimentally tested 6 kW_{el} IC cogeneration unit and evaluated its energy and exergy performance considering different Italian and Portuguese heat and electricity scenarios. The obtained primary energy saving was equal to 3% for Portugal, and 10% for Italy, respectively. Dorer and Weber [4] compared different CHP technologies (prime movers) integrated in single and multi-family houses of different energy standard levels. The simulations results obtained by using the simulation program TRNSYS indicate that most CHP systems offered reductions (up to 34%) in comparison with the gas boiler reference system and crediting the electricity exported to the grid. In Ref. [5] the CHP systems based on different prime movers (1 kW_{el} to 9 kW_{el}) were experimentally tested in residential application in Italy and Germany. According to the results a significant primary energy savings amount up to 27% and 36%, and a pollutant emissions reduction up to 33% and 35%, in Italy and Germany, respectively. Ciampi et al. [6] performed energy, environmental and economic dynamic simulations of a residential micro-cogeneration system of 6 kW_{el} in various Italian climatic zones. The best system performance was achieved for the coldest Italian city (Milan) for which the primary energy saving of 6.5%, a reduction of CO_2 equivalent emissions and operating costs of 12.8% and 29.9%, respectively, were ensured. Marrasso et al. [7] analyzed natural gas IC based cogeneration system (5.5 kW_{el}) on experimental and simulation basis. The system ensured a primary energy saving of 12.1% and a reduction of equivalent CO_2 emissions

equal to 27.8%. The payback period of the analyzed solution used to meet the electric and thermal demand of two residential buildings located in northern Spain, was equal to 11.9 years. Asaee et al. [8] conducted a preliminary techno-economic evaluation of retrofitting reciprocating IC engine based cogeneration into existing houses in five major climatic conditions of Canada for the purpose of achieving or approaching net-zero energy rating. In Ref. [9] the same authors performed a comprehensive techno-economic evaluation of retrofitting IC engine based cogeneration systems (3.87 kW_{el} to 25 kW_{el}) in the Canadian housing stock. The simulation results show that cogeneration retrofit yields 13% energy savings while the total GHG emissions would be reduced by 35%. Arbabi et al. [10] developed a numerical model to design and select a CHP unit based on an internal combustion engine. They concluded that several smaller engines in parallel mode is preferred over a single large engine due to longer operation period at full load operation and reliability level improvement.

Unfortunately there are practically no publications related to the techno-economic evaluation of IC based cogeneration systems in the Serbian climatic conditions using building energy simulation software. Using the model of residential building and the software EnergyPlus, the energetic and economical performance of IC based small scale cogeneration unit will be simulated and compared with performance of conventional systems. The purpose of this investigation is to gain a preliminary understanding of IC engine based cogeneration unit performance for the Serbian residential buildings and to identify the possible barriers for its widespread application. It is expected that this investigation will be very beneficial to those dealing with the design, analysis, simulation and energy performance assessment of IC engine cogeneration systems.

2. BUILDING MODEL

The selected building is a three-level student dormitory (Fig. 1). There are a total of twenty three bedrooms arranged on second and third level (Table 1). The dormitory provides accommodation and meals for students, as well as washing and drying services. A restaurant, kitchen, washing and drying service are located on the first level of the building. Restaurant services can also be used by those who are not accommodated in the dormitory.

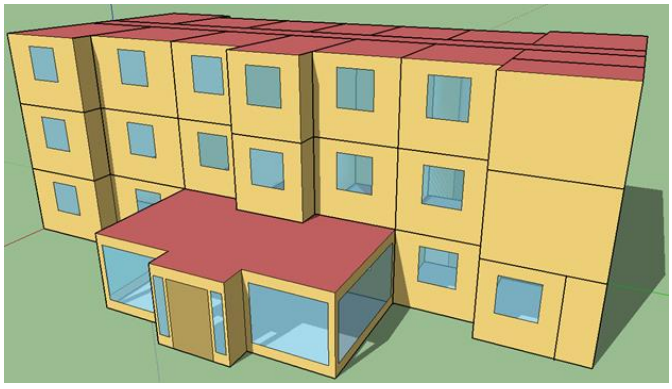

Figure 1. Isometric view of the analyzed student dormitory

The energy behaviour of the dormitory was simulated by using the EnergyPlus software (version 8.4.0) [11]. The EnergyPlus software takes into account all factors that influence

heat losses and loads in the building, such as electrical appliances, lighting, people occupancy, solar radiation, wind, infiltration and shading [12, 13]. The simulation was conducted for real weather data for the city of Kragujevac (Serbia). The people occupancy for bedrooms, toilets, bathrooms and restaurant is given in Table 1. The detailed yearly occupancy patterns (schedules) include people occupancy in the dormitory during the weeks (days) of lectures at faculties, the occupancy during the weeks of vacation, as well as the student occupancy in the dormitory during National holidays of the Republic of Serbia for 2017 [14]. It was assumed that the heat gain per person amounts 99 W, which is related to the activity of reading (seated) [15]. The occupancy schedules were defined according to the activities and behaviour of the students from nearby faculties, who are accommodated in the selected dormitory. The operation schedules for lighting correspond to the people occupancy schedules, with the difference when the lights are turned off during sleep and when the level of daylight is satisfactory.

Table 1. People occupancy and electric load in the dormitory rooms and restaurant

Room (total number)	Maximum people occupancy (-)	Power of lights (W)	Power of electrical appliances (W)
One bed room (2)	1	23	90
Three bed room (11)	3	27	270
Four bed room (10)	4	36	360
Bathroom (2)	4	18	-
Toilet (2)	4	18	-
Restaurant (1)	123	81	-

The highest electricity consumption within a dormitory is related to the electrical appliances located in kitchen. In order to simulate real operation of these appliances the electricity consumption data collected from fourteen UK public commercial kitchens were used [16]. All electricity consumption data for kitchens has been gathered exclusively from all cooking and food storage appliances, omitting any kitchen ventilation, washing or gas consuming appliances (Table 2).

Table 2. Average total daily electricity consumption for cooking, food storage, washing and drying appliances

	Walk in Fridges [16]	Walk in Freezers [16]	Other cooking appliances [16]	Combi-Ovens [16]
El. consu. (kWh)	13.81	39.17	6.08	35.71
	Other Refrigeration [16]	Clothes washers [17]	Clothes dryers [18]	Dishwashers [19]
El. consu. (kWh)	70.13	6	13.76	12.96

The values for electricity consumption for washing and drying appliances were taken from product catalogs. Four clothes washers and four dryers provide washing and drying of bed

sheets, while four dishwashers were used for dishwashing. It should be mentioned that electricity data given in Table 2 are related to the maximum people occupancy in the student dormitory. In other words, electricity consumption of cooking, food storage, washing and drying appliances correspond to the people occupancy.

3. DHW LOAD PROFILE

The shape and magnitude of DHW load of a student dormitory largely depends on number of students, their activity, time of day and time of year. Due to the absence of real load profile the DHW load profiles were determined according to the recommendations given in [20] and in Table 3. The total DHW consumption of dormitory represents the sum of consumption for all places (units) of consumption: bathrooms, restaurant, kitchen and laundry room. Both bathrooms are equipped with four showers and four wash basins. The hot water is used for maintaining personal hygiene (hand washing, showering, teeth brushing,..). It was assumed that half of the students take a shower in the morning and the other half in the evening. The adopted consumption of hot water with the desired temperature in bathrooms is given in Table 3. The only place in the restaurant where hot water is consumed is two wash basins (Table 3). They are used for hand washing before and after a meal. The maximum number of people that can use restaurant services in the same time is 123, of which 77 are students accommodated in the dormitory. The hot water consumption in the restaurant occurs three times a day, during breakfast, lunch and dinner.

The DHW consumption profile in the kitchen is more complex than the previously described profiles. In the kitchen, the consumption of DHW is related to the preparation of meals, hot drinks and dishwashing (Table 3). The highest consumption occurs during the lunch preparation and the least during the breakfast preparation.

The laundry service implies clothes and bed sheets washing for students accommodated in the selected dormitory (Table 3). The laundry room includes four washing machines, two of which are for clothes washing and the other two for bad sheets washing. The washing process performs twice during the evening.

Table 3. DHW consumption characteristics

Place of consumption		DHW consumption per person (l/person)	Duration (min)	Desired temperature (˚C)
Bathrooms	Wash basin	10	2	40
	Shower	50	6	40
Restaurant	Wash basin	5	1.5	40
Kitchen	Meal preparation	1	10	60
	Hot drink preparation	0.3	10	60
	Dishwashers	40 (l/washing)	30	60
	Wash basins	30 (l/washing)	10	60
Laundry room	Washing machines	188 (l/washing)	30	40

4. PLANT MODEL

Three different systems (cases) for DHW preparation were investigated (Fig. 2). The first case (System 1) is related to the internal combustion engine based cogeneration system with auxilary gas heater. The system with natural gas water heater represents the case 2 (System 2) and the system with electric water heater represents the case 3 (System 3). The only difference between the System 2 and 3 is in type of fuel used for DHW heating.

For the System 1 the thermal energy for DHW preparation is provided from lube oil system, jacket water cooling system and exhaust gas system. The water from the water storage tank (water heater) flows through the lube oil, jacket water and exhaust gas heat exchanger where it is heated. The heated water then circulates through the heat exchanger of the water storage tank where it transfers the heat to the water for DHW purposes. If the waste heat from engine systems is not enough to balance the DHW thermal load, auxiliary gas heater, within the storage tank, is turned on. When there is excess heat generated an excess heat exchanger is used to transfer engine heat to a surrounding.

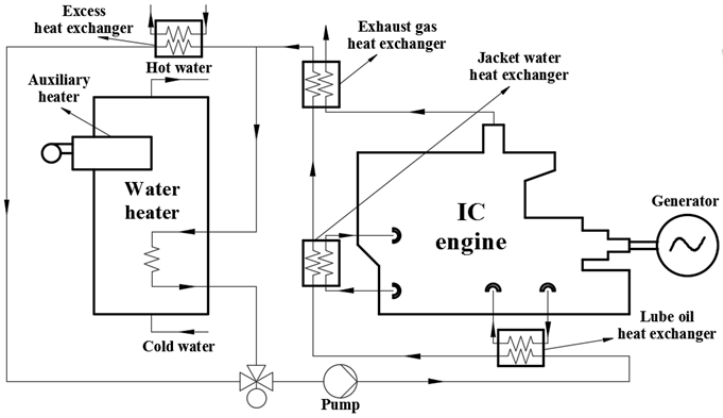

Figure 2. Internal combustion engine based cogeneration system (System 1)

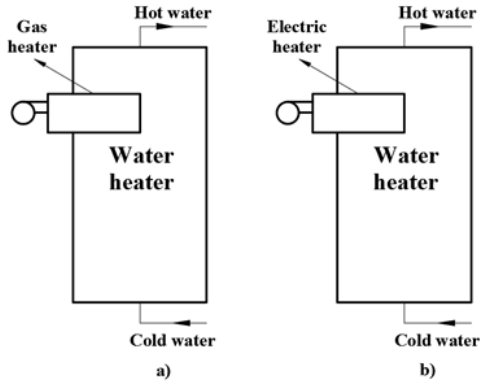

Figure 3. Conventional water heaters: a) gas water heater (System 2) and b) electric water heater (System 3)

The heat capacity (170 kW) and volume of the water heater (3200 l) are determined according to the DHW load profile and procedure described in [20]. The adopted values of the parameters needed for sizing of the water heater are given in Table 4.

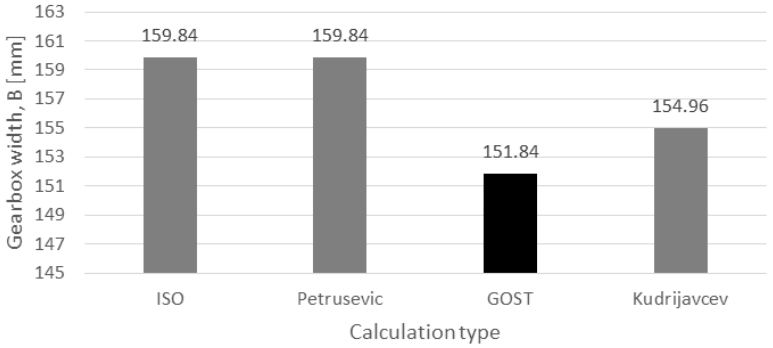

Figure 3. Gearbox widths

According to height criteria values corresponding to each design solution are given in Figure 4. The range of values is from 252.6 (Petrusevic) to 350 mm (Kudrijavcev). According to this criteria the most favourable solution is according to Petrusevic.

Table 4. The sizing parameters of the water heater

Parameter	Unit	Value
Maximum flow rate of the DHW during one hour	(l/s)	0.961
Minimum allowed temperature for water in water heater	(˚C)	10
Heat loss coefficient of the water heater	-	1.1
Thermal efficiency of the electric/natural gas heater	-	0.9
Number of hours for water heating	(h)	1
Number of hours for water heater operation	(h)	2
Maximum temperature for water in water heater	(˚C)	60
Factor due to unused space under the heating surface of the water heater	-	1.1

In order to determine the size of the cogeneration system it is necessary to know the daily, monthly or yearly profile of heat and electrical demands. For the selected student dormitory the IC cogeneration system is sized to provide minimum (base) thermal energy requirement for DHW preparation. In Fig. 4 the daily profile of heater heat capacity for the day of maximum heat demand is shown.

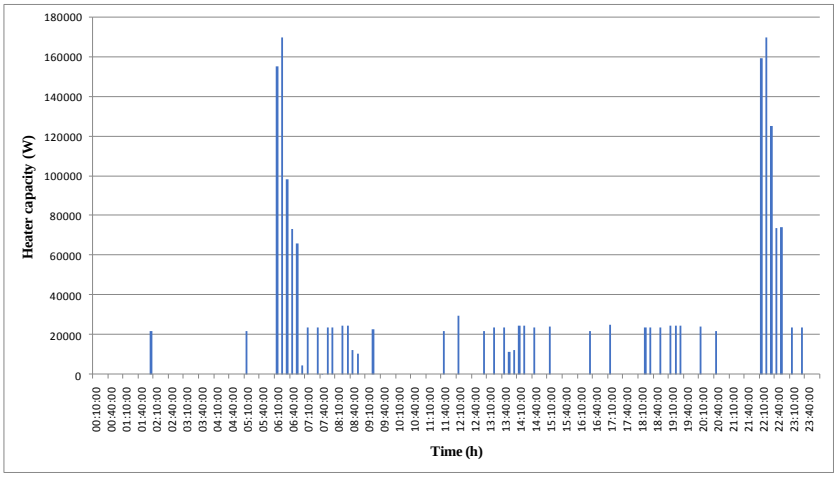

Figure 4. The daily profile of heat demands for DHW preparation

According to the data from Fig. 4 the daily share of heater heat capacity up to 25 kW amounts 76%, and over 25 kW amounts 24%. Based on this conclusion, the commercially available IC cogeneration unit, Viessmann Vitobloc 200 EM-9/20, has been adopted. Its technical characteristics are given in Table 5.

Table 5. Technical characteristics of the IC cogeneration unit Viessmann Vitobloc 200 EM-9/20 [21]

Load (%)	50	75	100
Electrical output (kW)	4.3	6.4	8.5
Thermal output (kW)	12.3	16.1	20.1
Fuel (natural gas) use (kW)	18.3	23.8	30.1
Electrical efficiency (%)	23.5	26.9	28.2
Thermal efficiency (%)	67.2	67.6	66.8
Maximum water temperature for heat recovery (˚C)	65		
Maximum exhaust gas temperature (˚C)	100		

The IC engine operates at full load at all times during the period from 6 a.m. to 11 p.m., to maintain the thermal storage tank water temperature of 60 ˚C. During the weeks of vacation and National holidays the cogeneration unit does not operate. The effect of engine start-up and shut-down losses are ignored in the simulations.

In order to simulate the energy behavior of the IC cogeneration system the empirical mathematical model available in the software EnergyPlus was used. The model which simulates the operation of a modified Otto engine, consists of performance curves which has to be generated by fitting catalog data to second order polynomial equations. Five performance curves were used: "shaft power" curve; "jacket heat recovery" curve; "lube heat recovery" curve; "total exhaust energy" curve and "exhaust temperature" curve.

The "shaft power" curve is a equation that is used to calculate the electrical output divided by the fuel energy input as a function of part load ratio:

$$\frac{E_C}{F_C} = \frac{E_C}{\dot{m}_{fuel} \cdot LHV} = a_1 + a_2 \cdot PLR + a_3 \cdot PLR^2 \quad (1)$$

where E_C is the engine electrical output (W); F_C is the fuel used by engine (W); $\dot{m}_{fuel}$ is the fuel mass flow rate (kg/s); LHV is the lower heating value of a fuel (J/kg); a_1, a_2, a_3 are coefficients (-) (a_1 = 0.004; a_2 = 0.644; a_3 = -0.371); PLR is the part load ratio of a engine (-) ($PLR = E_C/NE_C$, where NE_C is the rated electrical output of a engine (W)).

The "jacket heat recovery" and "lube heat recovery" curves are a quadratic equations that determine the amount of recovered jacket heat and recovered lube oil heat, respectively, as a function of part load ratio:

$$\frac{H_W}{F_C} = \frac{H_W}{\dot{m}_{fuel} \cdot LHV} = b_1 + b_2 \cdot PLR + b_3 \cdot PLR^2 \quad (2)$$

$$\frac{H_L}{F_C} = \frac{H_L}{\dot{m}_{fuel} \cdot LHV} = c_1 + c_2 \cdot PLR + c_3 \cdot PLR^2 \quad (3)$$

where H_W is the heat recovered from the jacket water cooling system (W); b_1, b_2, b_3 are coefficients (-) (b_1 = 0.2866; b_2 = 0; b_3 = 0); H_L is the heat recovered from the lube oil system (W) and c_1, c_2, c_3 are coefficients (-) (c_1 = 0.1719; c_2 = 0; c_3 = 0).

The amount of heat recovered by the exhaust gas heat exchanger is defined by the "total exhaust energy" and "exhaust temperature" curves. The exhaust gas temperature and flow rate are used if a stack heat exchanger is used to recover waste heat from the engine exhaust gas. This temperature is the inlet temperature to the heat exchanger. Both quadratic equations are in a function of part load ratio:

$$\frac{H_{EXH}}{F_C} = \frac{H_{EXH}}{\dot{m}_{fuel} \cdot LHV} = d_1 + d_2 \cdot PLR + d_3 \cdot PLR^2 \quad (4)$$

$$\frac{T_{EXH}}{F_C} = \frac{T_{EXH}}{\dot{m}_{fuel} \cdot LHV} = e_1 + e_2 \cdot PLR + e_3 \cdot PLR^2 \quad (5)$$

where H_{EXH} is the heat recovered from the exhaust gas system (W); d_1, d_2, d_3 are coefficients (-) (d_1 = 0.1965; d_2 = 0; d_3 = 0); T_{EXH} is the exhaust gas temperature (K) and e_1, e_2, e_3 are coefficients (e_1 = 373; e_2 = 0; e_3 = 0).

The coefficients a_1, a_2, a_3, b_1, b_2, b_3, c_1, c_2, c_3, d_1, d_2, d_3, e_1, e_2 and e_3 were generated according to the catalog data of the selected IC cogeneration unit [21]. It should be noted that for lower difference between the temperature of water leaving the exhaust heat exchanger and the temperature of water in water heater heat recovery amount will be lower. In that case the excess heat exchanger is activated in order to transfer the excess heat to a surrounding.

5. SIMULATION RESULTS AND ANALYSIS

5. 1 Energy amounts

Annual simulations of operation of all three investigated systems for DHW preparation were performed. The results of simulations were used to compare the performance of the IC cogeneration system (System 1) with conventional systems (System 2 and System 3). Fig. 5 presents the monthly energy consumption for DHW preparation of the analyzed systems. The energy consumption of the System 1 includes the gas consumption of IC engine and gas consumption of auxiliary heater (burner).

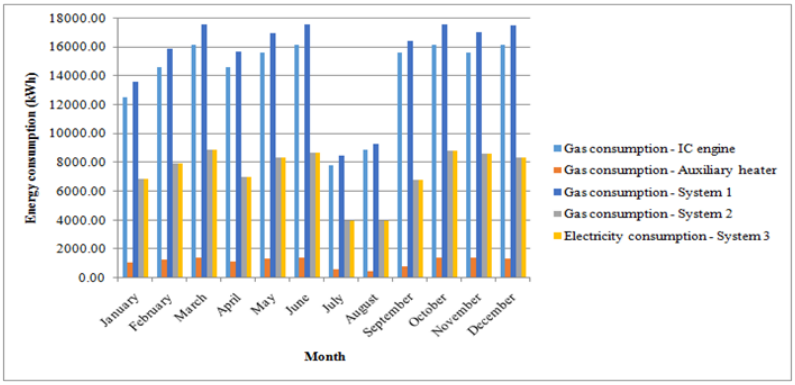

Figure 5. The monthly energy consumption for DHW preparation of the investigated systems: IC cogeneration system (System 1); Gas water heater (System 2); Electric water heater (System 3)

The energy consumption varies during the year, being different each month as a consequence of the people occupancy variation. In this respect, the highest energy consumption corresponds to the maximum people occupancy in the student dormitory, during March, June, October and December. On the other side, the minimum DHW loads and energy consumption were recorded during the weeks of vacation (July and August). It should be noted that the energy consumption for the gas and electric water heater (System 2 and System 3) is the same because the values of their thermal efficiency are equal (Table 4). Since, the IC cogeneration unit is dimensioned to cover the base thermal load the auxiliary burner provides additional thermal energy. The total yearly gas consumption of the IC engine amounts 170061.37 kWh while the consumption of the gas burner amounts 13526.75 kWh which represents 7.95% of the engine gas consumption. The yearly consumption of the System 2 and 3 is equal to 88234.44 kWh.

The monthly amounts of heat recovered by the lube oil, jacket water and exhaust gas heat exchangers are shown in Fig. 6. The total heat recovered from the IC cogeneration unit is 73665.52 kWh. The largest share of recovered heat of 47.3% is related to the jacket water, followed by share of 28.4% for lube oil and 24.3% for exhaust gas. As it was mentioned the amount of recovered heat is affected by the DHW needs and accordingly the temperature of the water inside the thermal storage tank.

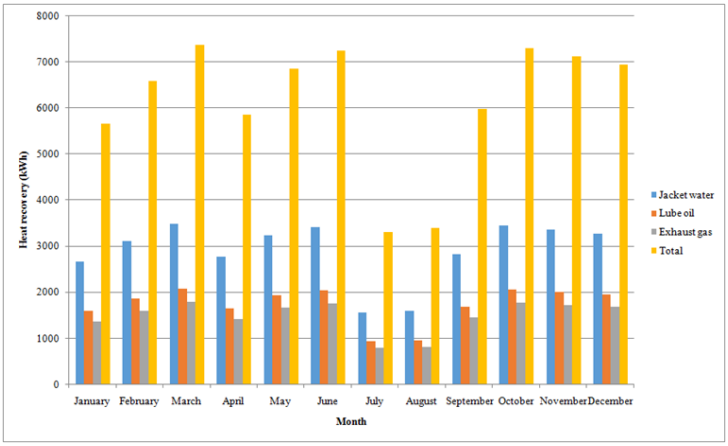

Figure 6. The monthly values of heat recovered from lube oil, jacket water and exhaust gas of IC cogeneration system

Fig. 7 presents the monthly electricity consumption and electricity production within the investigated student dormitory. The electricity is consumed by lighting and electrical appliances of the bedrooms, bathrooms, restaurant, kitchen, laundry and machine room. Due to the use of LED lights the electricity consumption for lighting is very low and almost negligible in relation to the consumption for electrical appliances. The amount of electricity consumption for electrical appliances is largely affected by the electric load and power of appliances located in the kitchen. The annual electricity consumption for lighting, appliances and entire student dormitory is 1126.24 kWh, 63546.95 kWh and 64673.19 kWh, respectively.

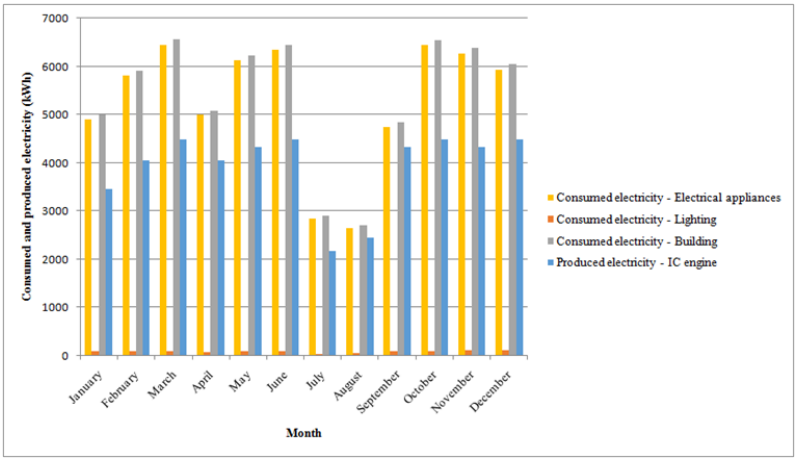

Figure 7. The monthly values of consumed and produced electricity within the student dormitory

The IC cogeneration system is in operation at full electrical load at all times during the period from 6 a.m. to 11 p.m. In this respect, the amount of electricity produced by the IC engine is the same for every day of its operation. The value of annual electricity production

of 47107 kWh covers 72.84% of the annual electricity consumption of the student dormitory. The highest cover (90%) is reached in August and September due to the significantly lower electricity consumption caused by lower people occupancy in the dormitory. According to the simulation results, the thermal and electrical efficiency of the simulated IC cogeneration system amounts 0.433 and 0.277, respectively. For the adopted and assumed value for the thermal and electrical efficiency of separate heat and electricity production of 0.9 and 0.3, respectively, the primary energy savings ratio (*PESR*) is equal to 28.81% while the total efficiency of the cogeneration unit is 0.71.

5.2. Energy costs

The costs of fuel consumption for investigated systems for DHW preparation has to be determined in order to analyze the economic feasibility of IC cogeneration system application. For the System 1 the costs are defined by summing the total fuel consumption of the IC engine unit and the fuel consumption of the auxiliary heater. Since the System 1 and System 2 use natural gas as fuel the fuel costs are calculated by dividing the fuel consumption by LHV of natural gas of 38.23 MJ/m^3 and then multiplying the consumption in cubic meters by the price of natural gas of 32.28 RSD/m^3 (1 € = 118.5 RSD).

The costs for electricity consumed by the System 3, lighting and electrical appliances are calculated by multiplying the amount of consumed electricity by the price of electricity which is defined according to the tariff payment system given in Table 6. The shown value of the electricity price does not include the taxes and levies.

Table 6. Tariff payment system for consumed electricity in Serbia (for two tariff electricity meter) [22]

Households	Higher daily tariff (RSD/kWh)	Lower daily tariff (RSD/kWh)
Green zone: 0 - 350 kWh	5.962	1.491
Blue zone: 350 - 1600 kWh	8.943	2.236
Red zone: over 1600 kWh	17.887	4.472

The tariff system consists of two tariff categories: higher daily tariff and lower daily or nightly tariff. The amounts of electricity consumed in both tariff categories are determined on the basis of operation schedules of DHW systems and electric equipment. For the operation of the System 1 and System 2 it was adopted that 85% of electricity is consumed during the duration of the higher tariff and 15% during the duration of the lower tariff category. On the other hand, when the System 3 is in operation the electricity is the only form of energy used in the student dormitory. Thus, the shares of consumed electricity are different and amount 60% (higher tariff) and 40% (lower tariff).

The easiest and the most commonly used economic indicator for analyzing financial attractiveness of a cogeneration project is the simple payback period ($SPB = F/S$). It presents the length of time (*SPB*), expressed in years, required to return investment costs (*F*). The parameter *S* denotes the annual net savings. According to the electrical output of the selected IC engine (8.5 kW) and estimated capital costs for IC cogeneration systems of various sizes, given in Table 7, the value for investment costs of 2800 \$/kW$_{el}$ was adopted.

Table 7. Estimated capital costs for IC cogeneration systems [1]

Cost Component	Senertec	North American Cogeneration Systems			MAN
Electrical Capacity (kW)	5.5	7.1- 10.7	20.1-23.3	30.3-35.0	100.0
Electrical Efficiency (%)	27	28.1	37.4	33.1	30.6
Thermal Efficiency (%)	61	56.5	50.0	51.2	50.4
Installed Cost ($/kW$_{el}$)	3020	2800	1600	1300	1080

The maintenance costs of the IC engine affect the value of the annual net savings *S*. These costs are related to the repair or replacement of engine components such as oil and air filters, spark plugs, gaskets, valves, piston rings and oil. They have been estimated to be 0.0105 $/kWhe [1].

The investment costs, annual fuel consumption (operating costs), maintenance costs and the annual savings for investigated cogeneration system for DHW preparation are presented in Table 8. In the same table the operating and maintenance costs for the other two analyzed systems (System 2 and 3) are shown and compared with the same for the System 1.

Table 8. Economic analysis of the IC based cogeneration system

	System 1	**System 2**	**System 1**	**System 3**
Costs				
Natural gas (RSD)	558054.1	268206.8	558054.1	-
Electricity - electric heater (RSD)	-	-	-	949516.95
Electricity - electric equipment (RSD)	829814.7	829814.7	829814.7	654506.62
Investment (RSD)	2451400	-	2451400	-
Operating and maintenance (RSD)	50946.2	-	50946.2	-
Total annual costs (RSD)	1438815.1	1098021.6	1438815.1	1604023.6
Savings				
Unconsumed electricity (RSD)	550955.81	0	550955.81	0
Total annual savings (RSD)	210162.34		716164.33	
***SPB* (years)**	11.66		3.42	

The *SPB* of the IC engine was calculated under assumption that the System 2 or the System 3 have been already installed in the student dormitory. From the comparison of the System 1 and 2 it can be concluded that the payback period of 11.7 years is relatively high. Accordingly, the selected IC cogenerated system can be considered as economically unsustainable. The investment costs and the low price of purchased electricity were found to be the main obstacles to implement the IC based cogeneration system. The capital costs per unit capacity of a cogeneration plant increase as the size of the plant is decreased (Table 7). The costs of the selected IC engine (8.5 kW$_{el}$) are 2.6 times higher than the capital costs for the engine with capacity of 100 kW$_{el}$. In this respect, the investment cost reduction in small scale cogeneration systems has to be achieved.

On the basis of the values of energy consumption and energy costs of the analyzed student dormitory the average price for purchased electricity amounts 12.83 RSD/kWh (10.83 c€/kWh). This electricity price does not support the application of IC based cogeneration plants. Comparing with the average electricity price in the European Union (for 28

countries) of 17.77 c€/kWh [23] and the average electricity price in Germany of 26.67 c€/kWh [23] it is relatively low. According to these prices and the average price of natural gas in the European Union (5.42 c€/kWh) [24] and Germany (5.44 c€/kWh) [24] the payback period would be 7.46 and 2.98 years, respectively.

The return of investment can be reduced by incentives in the form of subsidies and by implementation of the clean development mechanism (certified emission reduction). In order to encourage investors and reduce the investment risk the Government of the Republic of Serbia has adopted feed-in tariffs for different types of power plants which have obtain the status of the privileged electric power producers. The feed-in tariff for the combined heat and power generation is 8.89 c€/kWh [25]. If all produced electricity within a dormitory would be sold to the local company for electricity distribution for the mentioned price of 10.53 RSD/kWh (8.89 c€/kWh) the *SPB* would be even higher, 15.8 years. This leads to the conclusion that the existing value of the feed-in tariff is also disincentive. In order to achieve the payback period of 5 years, the value of 17.64 RSD/kWh (14.89 c€/kWh) for the price of sold electricity should be introduced. In other words, the average purchased electricity price has to be 37.5% higher while the feed-in tariff should be increased by 67.5%.

On the other hand, comparing the System 1 with the System 3 the parameter *SPB* is relatively low (3.42 years) due to the significantly high costs for electricity used for heating DHW (949516.95 RSD) by using the System 3. Although, for this case the implementation of IC based cogeneration unit is justified the water heating systems equipped with conventional electric heater are undesirable in terms of energy utilization efficiency because the overall conversion efficiency into thermal energy is relatively low.

6. CONCLUSIONS

In this paper the energetic and economic performance assessment of residential application of IC engine based cogeneration system in the Serbian climatic conditions using building energy simulation software was performed. The investigated residential building is a student dormitory. The simulations performed for real weather data for the city of Kragujevac (Serbia) include detailed annual operation schedules for lighting, electrical appliances and annual occupancy and DHW load patterns. For the selected student dormitory the IC engine is sized to provide minimum thermal energy requirement for DHW preparation. The performance of IC based system was compared with the performance of the two other conventional systems for DHW preparation: gas water heater and electric water heater. Comparing the IC based system with gas water heater the period required to return investment costs of IC engine is relatively high (11.7 years). The main barriers for widespread residential application of IC engine cogeneration system are related to the high capital costs and low price of purchased or sold electricity. The reduction of investment costs, by introducing incentive measures in the form of non-refundable funds in the appropriate percentage value of the investment costs would certainly contribute to the reduction of the payback period value and support development of small scale cogeneration systems. In relation to the current price in Serbia the price of purchased and sold electricity (feed-in tariff) should be higher by 37.5% and 67.5%, respectively, in order to achieve the value of payback period of five years. Comparing the IC based system with electric water heater the application of the IC based system is economically feasible since the payback period amounts 3.42 years. According to the simulation results, the IC engine cogeneration system ensured a primary energy saving of 28.81%. It should be noted that economic analysis does not include the interest rate, time value of money, as well as maintenance costs for System 2 and 3 which would certainly affect the payback period.

ACKNOWLEDGMENTS

This investigation is a part of the project TR 33015 of the Technological Development of the Republic of Serbia and project III 42006 of Integral and Interdisciplinary investigations of the Republic of Serbia. We would like to thank the Ministry of Education, Science and Technological Development of the Republic of Serbia for their financial support during this investigation.

REFERENCES

[1] Knight, I., Ugursal, V.I., "Residential cogeneration systems: a review of current technologies", A Report of Annex 42 of the International Energy Agency, Energy Conservation in Buildings and Community Systems Programme, 2005.

[2] Aussant, C.D., Fung, A.S., Ugursal, V.I., Taherian, H.: "Residential application of internal combustion engine based cogeneration in cold climate - Canada", Energy and Buildings, Vol. 41, No. 12, 2009, pp 1288-1298.

[3] Gonçalves, P., Angrisani, G., Roselli, C., Gaspar, A.R., Gameiro da Silva, M.: "Comparative energy and exergy performance assessments of a microcogenerator unit in different electricity mix scenarios", Energy Conversion and Management, Vol. 73, 2013, pp 195-206.

[4] Dorer, V., Weber, A.: "Energy and CO_2 emissions performance assessment of residential micro-cogeneration systems with dynamic whole-building simulation programs", Energy Conversion and Management, Vol. 50, No. 3, 2009, pp 648-657.

[5] Roselli, C., Sasso, M., Sibilio, S., Tzscheutschler, P.: "Experimental analysis of microcogenerators based on different prime movers", Energy and Buildings, Vol. 43, No. 4, 2011, pp 796-804.

[6] Ciampi, G., Rosato, A., Scorpio, M., Sibilio, S.: "Energy, Environmental and Economic Dynamic Simulation of a Micro-Cogeneration System Serving an Italian Multi-Family House", Energy Procedia, Vol. 78, 2015, pp 1141-1146.

[7] Marrasso, E., Roselli, C., Sasso, M., Picallo-Perez, A., Sala Lizarraga, J.M.: "Dynamic simulation of a microcogeneration system in a Spanish cold climate", Energy Conversion and Management, Vol. 165, 2018, pp 206-218.

[8] Asaee, S.R., Ugursal, V.I., Beausoleil-Morrison, I.: "Techno-economic evaluation of internal combustion engine based cogeneration system retrofits in Canadian houses - A preliminary study", Applied Energy, Vol. 140, 2015, pp 171-183.

[9] Asaee, S.R., Ugursal, V.I., Beausoleil-Morrison, I.: "An investigation of the techno-economic impact of internal combustion engine based cogeneration systems on the energy requirements and greenhouse gas emissions of the Canadian housing stock", Applied Thermal Engineering, Vol. 87, 2015, pp 505-518.

[10] Arbabi, P., Abbassi, A., Mansoori, Z., Seyfi, M.: "Joint numerical-technical analysis and economical evaluation of applying small internal combustion engines in combined heat and power (CHP)", Applied Thermal Engineering, Vol. 113, 2017, pp 694-704.

[11] Crawley, D.B., Lawrie, L.K., Winkelmann, F.C., Buhl, W.F., Huang, Y.J., Pedersen, C.O., Strand, R.K., Liesen, R.J., Fisher, D.E., Witte, M.J., et al.: "Energyplus: creating a new-generation building energy simulation program", Energy and Buildings, Vol. 33, No. 4, 2001, pp 319-331.

[12] Bojić, M., Nikolić, N., Nikolić, D., Skerlić, J., Miletić, I.: "Toward a positive-net-energy residential building in Serbian conditions", Applied Energy, Vol. 88, No. 7, 2011, pp 2407-2419.

[13] Lukić, N., Nikolić, N., Timotijević, S., Tasić, S.: "Influence of an unheated apartment on the heating consumption of residential building considering current regulations - case of Serbia", Energy and Buildings, Vol. 155, 2017, pp 16-24.

[14] Nikolić, N., Lukić, N., Dagović, V., Nešović, A., Matejić, M.: "Impact of the methods of occupancy schedule defining on people heat gains within a student dormitory", 49th International Congress and Exhibition on Heating, Refrigeration and Air-conditioning, Belgrade, Serbia, 2018, 5th-7th of December, pp 207-216.

[15] ASHRAE Handbook of Fundamentals, ASHRAE, Atlanta, 2005.

[16] Mudie, S., Essah, E.A., Grandison, A., Felgate, R.: "Electricity use in the commercial kitchen", International Journal of Low-Carbon Technologies, Vol. 11, No. 1, 2016, pp 66-74.

[17] Gorenje, Clothes washer, Technical Data. Available: https://partners.gorenje.com/fts/PiPki.aspx?ident=729291&jezik=sr [Accessed: 10/01/2019].

[18] Gorenje, Clothes dryer, Technical Data. Available: https://partners.gorenje.com/fts/PiPki.aspx?ident=730016&jezik=sr [Accessed: 10/01/2019].

[19] Candy, Dishwasher, Technical Data. Available: http://www.candy.rs/sr_RS_latin/aparati/operi-ososi/sudomasine/-/catalog/21698127/cdpm-77735 [Accessed: 10/01/2019].

[20] Recknagel, H., Sprenger, E., Schramek, E.-R.: "Taschenbuch für Heizung und Klimatechnik", R. Oldenbourg Industrieverlag GmbH, München, 2011.

[21] Viessmann, IC cogeneration unit, Technical Data. Available: https://www.viessmann.de/de/wohngebaeude/kraft-waerme-kopplung/blockheizkraftwerk/vitobloc-200-em-9-20.html [Accessed: 30/01/2019].

[22] EPS. Electricity prices in the Republic of Serbia. Available: http://www.eps-snabdevanje.rs/kupci/Documents/20170828_Odluka%20o%20regulisanoj%20ceni%20EE%20na%20garantovanom%20snabdevanju%2001.10.2017.pdf [Accessed: 16/02/2019].

[23] Eurostat. Electricity prices for household consumers. Available: http://appsso.eurostat.ec.europa.eu/nui/show.do?dataset=nrg_pc_204&lang=en [Accessed: 16/02/2019].

[24] Eurostat. Gas prices for household consumers. Available: http://appsso.eurostat.ec.europa.eu/nui/show.do?dataset=nrg_pc_202&lang=en [Accessed: 16/02/2019].

[25] Feed in tariffs in the Republic of Serbia. Available: https://www.energetskiportal.rs/ministarstvo/fid-in-tarife/ [Accessed: 18/02/2019].

Intentionally blank

MOBILITY & VEHICLE MECHANICS

DOI: 10.24874/mvm.2019.45.02.04
UDC: 629.047.14

THREE DIMENSIONAL ANALYSES OF SEAT BELT AND DRIVER IN CASE OF SUDDEN BRAKING

Slavica Mačužić [1*], *Igor Saveljić* [2]

Received in November 2018 Revised in December 2018 Accepted in February 2019

RESEARCH ARTICLE

ABSTRACT: A seat belt is a vehicle safety device designed to secure the occupant of a vehicle against harmful movement that may result during a collision or a sudden stop. In recent years, serious and fatal accidents have decreased in number. The reason is that more and more people begin to understand the importance of using safety belts. When driver makes a sudden stop, the speed from the car causes driver to hit the seat belt with significant force. That force saves life, but can leave passenger with bruises, scrapes and fractures. In this paper the influence of different force values on the abdomen of the driver by the seat belt is analyzed. As a result, the different speed values of the car, due to sudden braking, give different values of force which the seat belt acts on the driver.

KEY WORDS: driver, injury, vehicle, finite element method

[1]*Slavica Mačužić, Assistent, University of Kragujevac, Faculty of Engineering, Sestre Janjić 6, 34000 Kragujevac, Serbia, s.macuzic@kg.ac.rs (*Corresponding author)*
[2]*Igor Saveljić, PhD, University of Kragujevac, Faculty of Engineering, Sestre Janjić 6, 34000 Kragujevac, Serbia, isaveljic@kg.ac.rs*

TRODIMENZIONALNA ANALIZA POJASA I VOZAČA U SLUČAJU IZNENADNOG KOČENJA

REZIME: Sigurnosni pojas je sigurnosni uređaj vozila dizajniran da osigura putnika u vozilu od štetnog kretanja koje može nastati tokom sudara ili iznenadnog zaustavljanja. Poslednjih godina broj teških i fatalnih nesreća se smanjio. Razlog je taj što sve više ljudi počinje da shvata važnost korišćenja sigurnosnih pojaseva. Kada vozač naglo zaustavi, brzina od automobila dovodi vozača o značajnog udara u sigurnosni pojas. Ta sila spašava život, ali može ostaviti putnika modricama, ogrebotinama i lomovima. U ovom radu analiziran je uticaj različitih vrednosti sile na abdomen vozača pomoću sigurnosnog pojasa. Kao rezultat toga, različite vrednosti brzine vozila, usled naglog kočenja, daju različite vrednosti sile koje sigurnosni pojas deluje na vozača.

KLJUČNE REČI: vozač, povreda, vozilo, metoda konačnih elemenata

THREE DIMENSIONAL ANALYSES OF SEAT BELT AND DRIVER IN CASE OF SUDDEN BRAKING

Slavica Mačužić, Igor Saveljić

1. INTRODUCTION

Traffic accidents are a major source of fatalities and serious injuries [1]. The major cause of car occupant fatalities in car accidents is head injuries which occurs when vehicle passengers are thrown out through the windshield or when they collide with the vehicle seat or dashboard. Based on research the World Health Organization [2] injury in road traffic crashes is expected to become the third most important cause of the global burden of injuries/diseases by 2020. More than 1.25 million people die each year as a result of road traffic accidents. Globally, road traffic crashes are a leading cause of death among young people, and the main cause of death among those aged 15–29 years (Figure 1).

Based on all the research, a lot of effort has been invested to change the awareness of drivers and all passengers in vehicles. The most important form of passenger protection in the car is the use of the seat belt. Seat-belts limit the movement of vehicle occupants in the event of a crash in order to reduce the force that currently operates on the passenger in the vehicle. Wearing a seat-belt reduces the risk of a fatality among drivers and front-seat occupants by 45–50%, and the risk of minor and serious injuries by 20% and 45% respectively. In the case of passengers in the rear seat, the use of seat belts reduces fatal and serious injuries by 25% and minor injuries by up to 75% [3]. Over time, there is progress and development of awareness about the application of good laws in the binding of seat belts, but still only half of the country's world has adopted a good seat-belt laws. About 4.8 billion people, from 105 countries have seat belts in the back seat.

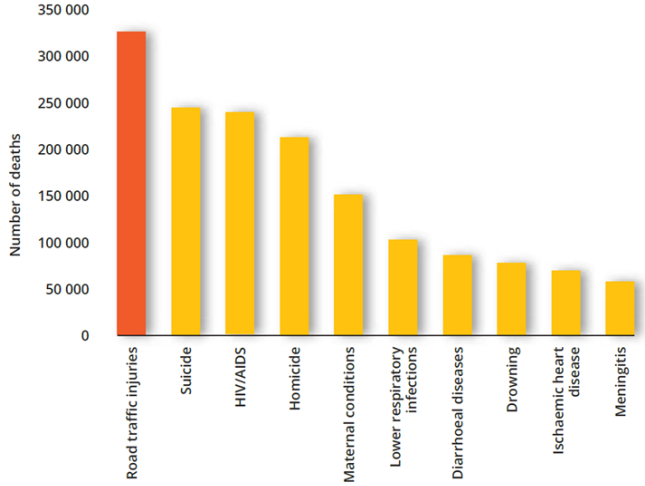

Figure 1. The most common causes of death of young people under 30 years [2]

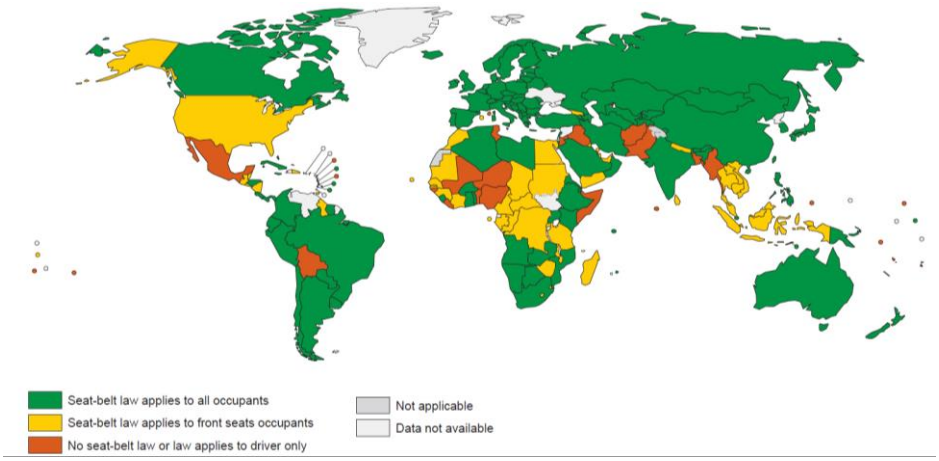

Figure 2. Seat-belt laws in the world

Experience from developed countries indicates that the use of seat belts is one of the most effective ways to reduce road accident fatalities [4, 5]. In this paper, using numerical simulations, it has been shown that the force of the sudden braking extends through the torso of an adult male person, previously tied to the safety belt.

2. MATERIALS AND METHODS

The finite element model of a human torso was developed using the CT scans. The high resolution CT data were read into Mimics 14.0 ((Materialise Inc., Leuven, Belgium) visualization software, where the images were segmented by thresholding to obtain 3D model (Figure 3).

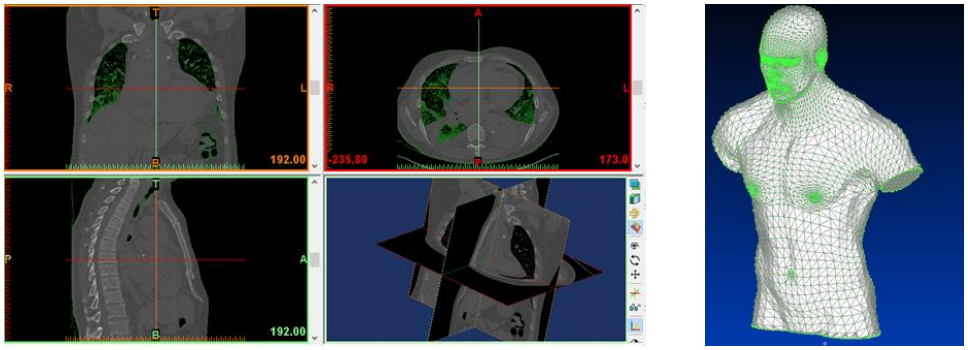

a) b)

Figure 3. The process for the 3D FE model: a) CT scan and 3D reconstruction of the CT scans, and b) meshing of the 3D FE model

The whole FE torso model was divided into two parts, including thoracic and abdominal soft tissues and thoracic cage (Figure 4). In this paper, the aim was to examine the values of the

load on the chest, and the pressure forces, so we did not take into account the human internal organs.

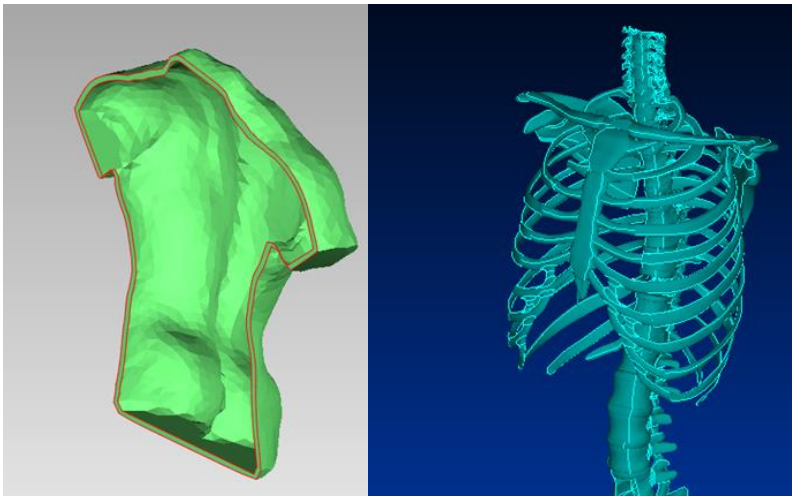

Figure 4. Finite element model of the human torso with tissue and thoracic cage

The material properties assignment is detailed in Table 1.

Table 1. Material properties of used materials

Parts	Material type	Parameters	Reference
Rib (cortical)	Elastic	$\rho = 2.0$ g/cm^3, E = 11.5 GPa, $\mu = 0.3$	[6]
Rib (trabecular)	Elastic	$\rho = 1.0$ g/cm^3, E = 0.04 GPa, $\mu = 0.45$	[6]
Tissue	Elastic	$\rho = 1100$ kg/mm^3, E = 10 MPa, $\mu = 0.3$	[7]

In this paper the model of an adult man weighing 85 kg, height 180 cm was used. Three cases of speed of car movement and sudden shock of an irreversible obstacle were analysed. The speed of the car was 40, 50 and 60 km/h. Also, the driver used the seat belt. According to [9], the following force values applied to the driver were used: 24.7 kN, 38.5 kN and 55.5 kN, for 40, 50 and 60 km/h, respectively.

One of the basic principles of continuum mechanics is the principle of virtual work. Starting from the equilibrium equations [8] by applying the boundary conditions can be equal to the virtual work of internal and external forces:

$$\delta W_{\text{int}} = \delta W_{ext} \tag{1}$$

Virtual work of the previous equation in matrix form can be written as:

$$\delta W_{\text{int}} = \int_V \delta \mathbf{e}^T \boldsymbol{\sigma} dV \qquad \delta W_{ext} = \int_V \delta \mathbf{u}^T \mathbf{F}^V dV + \int_{S^\sigma} \delta \mathbf{u}^T \mathbf{F}^S dV + \sum_i \delta \mathbf{u}^T \mathbf{F}^{(i)} \tag{2}$$

Applying the principle of virtual work and the constitutive relations for linear elastic material in matrix form

$$\boldsymbol{\sigma} = \mathbf{C}\mathbf{e} \tag{3}$$

and by applying the concept isoparametric interpolation [9] in the finite element, on the basis of which the coordinates and displacements at any point within the element is

$$\mathbf{x} = \mathbf{N}\mathbf{X} \qquad \mathbf{u} = \mathbf{N}\mathbf{U} \tag{4}$$

we can write the equation of equilibrium finite elements:

$$\mathbf{K}\mathbf{U} = \mathbf{F}_{ext} \tag{5}$$

where **K** is element stiffness matrix, **B** - strain relation matrix - displacements at the nodes, which contains excerpts interpolation function, **C** - elastic constitutive matrix, **e** = BU - matrix deformation, **U** - displacements at the nodes, **X** - coordinates of nodes, **N** - matrix of interpolation functions, $\mathbf{F}_{ext}$ - external forces in the element nodes.

In the linear analysis of solids a basic assumption is that the moving solids are infinitesimally small and that the material is linearly elastic. Also, the assumption is that the nature of the boundary conditions remains unchanged under the action of external loads. Under these assumptions, the equations of equilibrium are derived for finite element structural analysis. Equation (5) is related to the linear analysis of solids because the moving U is linear function of external forces $\mathbf{F}_{ext}$. In the case when displacement is not linearly dependent of the load, nonlinear analysis is applied.

In the linear analysis, the assumption that the displacement must be small is applied in calculating the stiffness matrix and force vector because all the volume integrals are applied to the original volume of the finite elements. Also, the matrix **B**, which relates strain and nodal displacement is constant for each element and is independent of the displacement element nodes. For a linear elastic material is assumed that the constitutive matrix is constant. Fixed boundary conditions are also the default in the linear analysis.

3. RESULTS

Numerical simulation was performed using the Ansys software package 14.5. Three cases of speed of car movement and sudden shock were analyzed. The speed of the vehicle was 40, 50 and 60 km/h. Following force values applied to the driver were used: 24.7 kN, 38.5 kN and 55.5 kN, for 40, 50 and 60 km/h, respectively. Figure 5 represent the results of the first simulation.

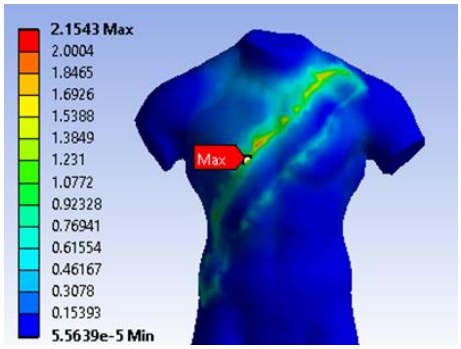

Figure 5. The numerical result of the von Misses stress when a force of 24.7 kN was applied on the chest part

The result of this simulation shows that the highest stress occurs on the chest part, due to the influence of the belt, where the maximum value was 2.15 MPa. Figure 4 and 5 shows the stress distribution for the remaining cases.

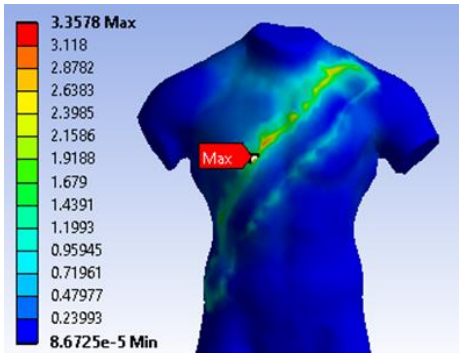

Figure 6. The numerical result of the von Misses stress when a force of 38.5 kN was applied on the chest part

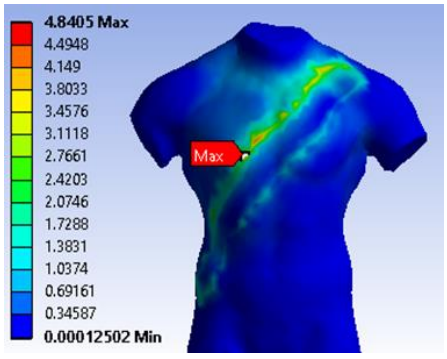

Figure 7. The numerical result of the von Misses stress when a force of 55.5 kN was applied on the chest part

From the previous figures, Figure 6 and Figure 7, it can be concluded that the maximum value of the stress is always in the chest. The highest stress values of the last two measurements are 3.35 and 4.84 MPa, respectively. It can be concluded that the dependence of force and stress is rather linear (Figure 8).

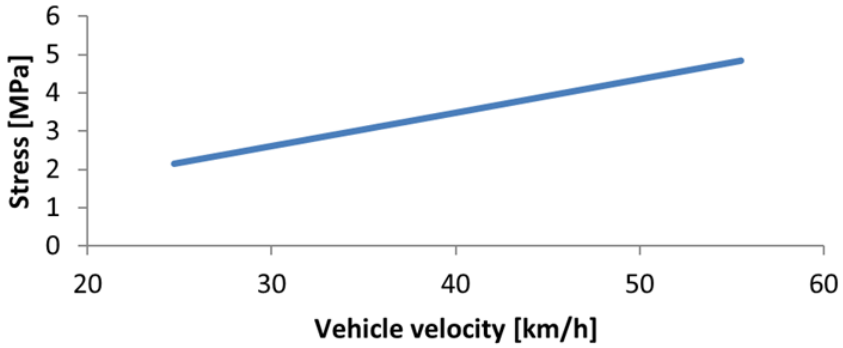

Figure 8. A diagram of the dependence of force and stress generated on the body of the model

4. CONCLUSIONS

Previous section shows the research results of the numerical simulation driver interactions and seat belts during a sudden impact on a fixed obstacle. Numerical simulations were done using Ansys 14.5 was used. Finite element model of the human torso with tissue and thoracic cage was used. Three cases of speed of car movement and sudden braking of an irreversible obstacle were analysed. The speed of the car was 40, 50 and 60 km/h. Also, the driver used the seat belt. The following force values applied to the driver were used: 24.7 kN, 38.5 kN and 55.5 kN, for 40, 50 and 60 km/h, respectively. The results of this study show where the greatest pressure on the human body was during sudden braking. The largest load zone is the upper part of the chest, where the values of the von Misses stress reach the highest values of 4.84 MPa, for the speed of a car of 60 km/h.

The direction of future research will be to investigate how internal organs suffer from sudden pressure, as well as the way the shifts affect them.

ACKNOWLEDGMENTS

This research supported by the Ministry of Education, Science and Technological Development of Republic of Serbia through Grant TR 35041.

REFERENCES

[1] World Health Organization: "United Nation road safety collaboration: a handbook of partner profiles", Geneva: WHO, 2005, pp 1-5.

[2] World Health Organization: "World report on road injury prevention", Geneva: WHO, 2005, pp 37-39.

[3] Elvik, R.: "The handbook of road safety measures", 2nd ed. Bingley, UK: Emerald Group Publishing Limited, 2009.

[4] Canada: crash modes and kinematics of injury, Accident Analysis and Prevention Journal 26, 1994, pp 207-214.

[5] Evans, L.: "Safety-belt effectiveness: The influence of crash severity and selective recruitment", Accident Analysis and Prevention Journal, Vol. 28, No. 4, 1996, pp 423-433.

[6] Li, Z., Kindig, M.W., Kerrigan, J.R., Untaroiu, C.D., Subit, D.: "Rib fractures under anterior–posterior dynamic loads: Experimental and finite- element study", Journal of Biomechanics, Vol. 43, No. 2, 2010, pp 228–234.

[7] Lizee, E., Robin, S., Song, E., Bertholan, N., Lecoz, J.Y., Besnault, B., Lavaste, F.: "Development of 3D Finite Element Model of the Human Body", SAE Transactions, SAE Paper number 983152, 1998, pp 2760–2782.

[8] Kojic, M.,

[9] Filipovic, N., Stojanovic, B., Kojic, N.: "Computer Modeling in Bioengineering - Theoretical Background, Examples and Software" John Wiley and Sons, Chichester, England, 2008.

[10] Bathe, K.J.: "Finite Element Procedures", Prentice-Hall, Inc., Englewood Cliffs, N.J, 1996.

Intentionally blank

MOBILITY & VEHICLE MECHANICS

DOI: 10.24874/mvm.2019.45.02.05
UDC: 534.1

PLATFORM OSCILLATIONS UNDER THE INFLUENCE OF INTEGRATED WEAPON'S RECOIL FORCE

Nina Živanović [1], Gordana Bogdanović [2]*

Received in October 2018 Accepted in December 2018

RESEARCH ARTICLE

ABSTRACT: Oscillations of light wheeled vehicle's centre of gravity, caused by firing weapon integrated on it, are studied through simulation of its axial and angular displacements. Dynamical model of system with three degrees of freedom is used and mathematical model of oscillations is defined using the Lagrange's equations of second order. Weapon recoil force and resistance force that causes vehicle's oscillations is calculated according to the internal ballistics data of integrated weapon and chosen system construction. System of differential equations is numerically solved in MATLAB for real firing conditions and vehicle configuration. Coordinates of weapon mount and elevation and azimuth angles are varied and results are analyzed.

KEY WORDS: oscillations, dynamical model, wheeled vehicle, integrated weapon

[1]*Nina Živanović, MSc, Military technical institute, Ratka Resanovića 1, 11000 Belgrade, nina.zivanovic.kg@gmail.com (*Corresponding author)*
[2]*Gordana Bogdanović, PhD Assoc. prof., University of Kragujevac, Faculty of Engineering, Kragujevac, Sestre Janjić 6, gocab@kg.ac.rs*

OSCILACIJE PLATFORME IZAZVANE SILOM TRAZAJA INTEGRISANOG ORUŽJA

REZIME: Oscilacije težišta lakog vozila točkaša nastale delovanjem oružja integrisanog na vozilo analizirane su simulacijom linijskih i ugaonih pomeranja. Korišćen je dinamički model sistema sa tri stepena slobode koji je matematički modeliran pomoću Langraževih jednačina druge vrste. Sila trzaja oružja i sila otpora koje izazivaju oscilacije vozila određene su na osnovu podataka dobijenih iz unutrašnje balistike integrisanog oružja i izabrane konstrukcije sistema. Sistem diferencijalnih jednačina je numerički rešen u MATLAB-u za realne uslove paljbe i koncepcije vozila. Varirane su vrednosti koordinate tačaka oslanjanja oružja, elevacije i azimuta variraju i analizirani su dobijeni rezultati.

KLJUČNE REČI: oscilacije, dinamički model, vozilo točkaš, integrisano oružje

PLATFORM OSCILLATIONS UNDER THE INFLUENCE OF INTEGRATED WEAPON'S RECOIL FORCE

Nina Živanović, Gordana Bogdanović

1. INTRODUCTION

Systems composed of light mobile platform with integrated weapon rise interest over the past few years because modern warfare require light military vehicles in the arsenal, with few crew members, efficient, not too expensive, intended for scouting, quick actions, neutralization and instant prevention of hostile forces.

Well-equipped armies have purpose-designed tactical vehicles, while less developed countries and paramilitary forces use improvised, already available, adapted vehicles. As a mobile platform, modified light commercial vehicle on wheels is most commonly used (pickup vehicles, utility vehicles). Besides the basic purpose, it also has to absorb additional load from weapon's recoil force. For this paper, Land Rover Defender 110 is selected as a mobile platform and automatic grenade launcher 30 mm caliber M93 as a weapon for integration.

Mathematical-mechanical model of system's oscillations was set based on theoretical approach for studying vehicle dynamics and differential equations of motions were derived. Referring to internal-ballistic data for weapon and vehicle construction parameters, specific equations of platform oscillations are acquired, which can be numerically solved in one of contemporary software packages.

Simulation, which is actually process of solving previously set equation system, is performed in MATLAB environment, giving the graphical representation of results, in this case system oscillations. With initial parameters variations, system precision and alteration of oscillations can be perceived.

2. WEAPON INTEGRATION ON PLATFORM

Weapon can be integrated on several places on the vehicle – it can be mounted on one of the reinforcing bars in the vehicle trunk, between the front seats, above the engine compartment, in front of the passenger seat or in some other place where crew members can operate it from. One of the simplest mounts is vertical bar fastened to vehicle floor. This kind of integration allows specified weapon elevation and azimuth adjustments, while the weapon remains fixed in the same place. More flexible solution is swing arm mechanism composed out of several axles ('arms'), which can cover up to 180° degrees along the horizontal direction. There are also mechanisms as 360-degrees turret mounts allowing weapon 360° degrees rotation.

Common practice is to mount weapon in the longitudinal vertical symmetry plane, or as close to it as manageable, so destabilizing moments are the smallest possible. Vehicle has a specific task to carry out when weapon is mounted on it – beside the loads transferred from the road, it has to withstand and absorb weapon generated loads. Main problems for this are inadequate stiffness of the vehicle chassis, adverse oscillations, low weapon firing precision etc. To fulfil these demands and solve occurring problems, the most important thing is to integrate weapon in optimal place and to provide suitable vehicle suspension system which can absorb loads, reduce oscillations and prevent resonance from happening.

2.1 Force transferred to the platform calculation

Automatic grenade launcher 30 mm M93 (Figure 1) was developed from Russian AGS-17 and uses blowback as operating principle.

Main targets of automatic grenade launchers are unsheltered troops or lightly sheltered targets and lightly armored vehicles. Those are convenient for mounting on military vehicles, boats and helicopters [1].

Figure 1. Automatic grenade launcher 30 mm M93

In Table 1 technical data for automatic grenade launcher 30 mm M93 are given.

Table 1. Technical data for AGL 30 mm M93 [2]

Data	AGL 30 mm M93
Empty weapon mass	35 kg
Bullet mass	0,360 kg
Effective firing range	1700 m
Vertical field of action	(-5°) ÷ (+70°)
Horizontal field of action	No tripod movement - 30°, with tripod movement - 360°
Muzzle velocity	185 m/s
Maximum pressure in barrel	$150 \cdot 10^6$ Pa

Within the simulation, internal-ballistic calculation [3] based on Drozdov method had been done and acquired values of maximum pressure in the barrel ($\boldsymbol{p_{max}} = 141{,}7$ MPa) and projectile muzzle velocity ($\boldsymbol{v_0} = 186{,}4$ m/s) were used as initial parameters for further computation. Obtained values barely deviate from the real ones.

Working principle of AGL is simple blowback, which obtains energy, used to perform automatic operation of a weapon, from residual pressure of propellant gasses. Motion of the parts is slowed by the mass of the bolt and the force required to compress the action spring [4]. In automatic grenade launcher 30 mm M93 internal friction force, spring resistance

force and hydraulic resistance force oppose to the motion of the recoil mass. Those forces together compose total force of resistance to recoil R [N], the force that is transferred to the platform and calculated according to the next equation:

$$R = F_{tr} + 2 \cdot F_{op} + F_{hk} - m_t \cdot g \cdot \sin \alpha \tag{1}$$

Figure 2 shows all of the resistance forces which occur during recoil process over time, as well as the total force of resistance to recoil.

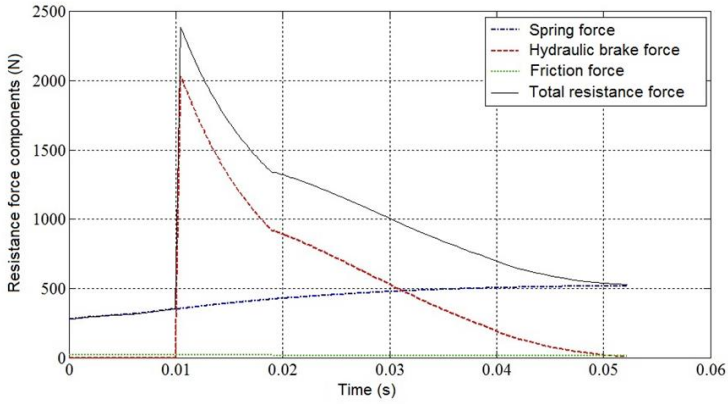

Figure 2. Resistance forces and total force of resistance to recoil

Hydraulic brake absorbs the most of recoil mass' kinetic energy, ca. 80%, so it has the biggest impact on R force change [5]. Maximum value of total force of resistance to recoil is $\mathrm{R_{max}} = 2385{,}9$ N, selected for further calculation.

3. INTEGRATING AGL 30 MM ON SELECTED LIGHT MOBILE WHEELED PLATFORM

Decision was made to mount automatic grenade launcher on the rooftop of the Land Rover Defender in the area above the back seat. Created model had to be simplified, but sufficiently accurate replacement for the real and complex system. Chosen simplified model has three degrees of freedom – translation of mass centrum in the direction of vertical axis *z* (T_z) and rotations around longitudinal *x* and lateral *y* axis (roll R_x and pitch R_y).

From a constructive point of view, simplifications include integration of weapon on the vehicle's longitudinal axis, solid link between them, not deforming construction, assumption that the system behaves as a compact mass, equal spring stiffness coefficients c_{ij}, as well as equal damping coefficients of front and back shock absorbers k_{ij}.

When weapon fires, resistance force to recoil R transfers to elastically suspended platform and causes system to oscillate, which makes it an excitation that takes the system out of

equilibrium position. With cessation of excitation system continues to oscillate, damped using shock absorbers, until it stops in equilibrium position.

In Figure 3 system scheme is shown, observed in *xz* plane, in right-hand oriented, stationary, perpendicular coordinate system attached to the ground (*xyz*). Coordinate system *x'y'z'*, attached to the system mass centrum *T*, moves with the system, a and b are distances from vertical axes of front and back vehicle axles, H_T is height of the mass centrum measured from the ground. Driving force operates in the point *D*, which position is defined by d and h distances from system mass centrum *T* in *z'x'* plane.

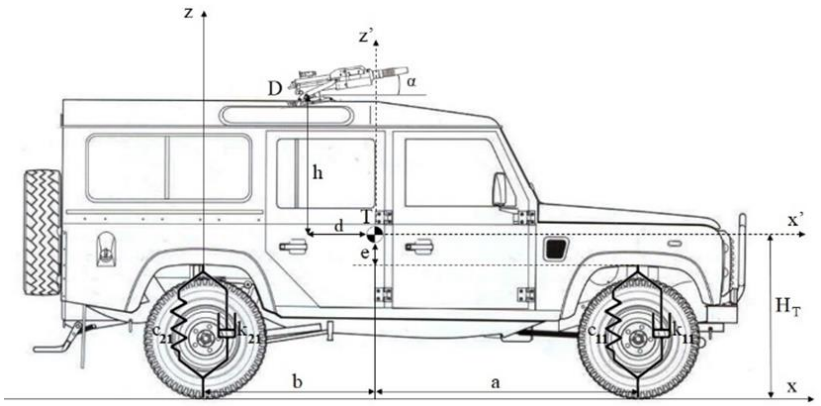

Figure 3. Simplified system scheme in the zx plane

In Figure 4 the same system is shown, observed from the front in the *z'y'* plane. Labels *s* are distances from system mass centrum *T* to left and right wheel vertical axes.

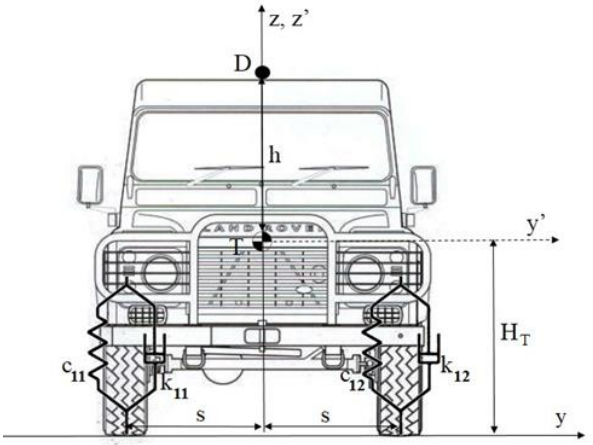

Figure 4. Bi–fuel systems (CNG or biogas) on passenger vehicle Volvo S80

In z'x' plane (Figure 5) side of the system is observed, translation in the z' axis direction, one of the front wheels and one of the back wheels, as well as rotation around y' axis (pitch) for angular displacement φ, in the arbitrary point in time.

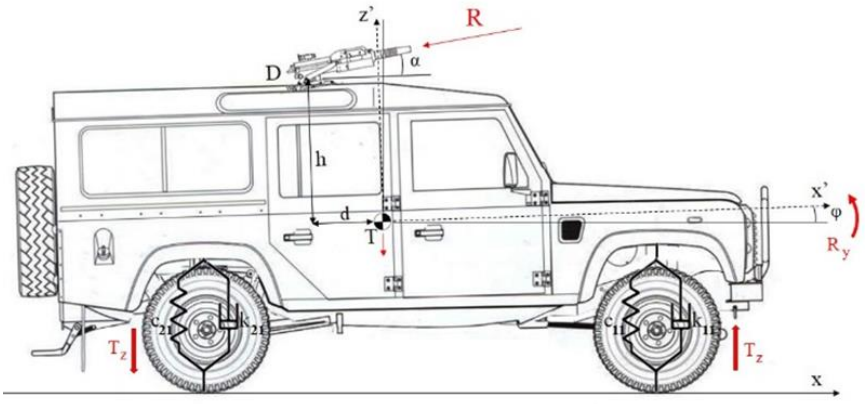

Figure 5. System model in the arbitrary point in time during the driven oscillation in zx plane

In the *z'y'* plane (Figure 6) system is observed from the front, vertical translation and rotation around *x'* axis (roll) for angular displacement *θ*, also in the arbitrary point in time.

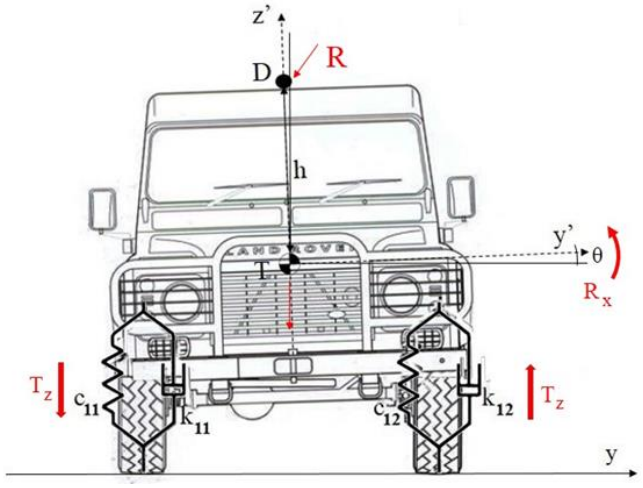

Figure 6. System model in the arbitrary point in time during the driven oscillation in yz plane

For simulation, weapon was fired from top of the stationary vehicle, elevation and azimuth angles defined in advance. For simplified model, differential equations as a description of system's motion were set.

4. MATHEMATICAL-MECHANICAL MODEL OF MOBILE PLATFORM OSCILLATIONS UNDER THE IMPACT OF WEAPON'S RECOIL FORCE

Mathematical-mechanical model represents movement of the physical system based on the classical principles of vehicle dynamics theory and includes all main influencing parameters [6]. Considering adopted simplifications, system with infinite number of degrees of freedom is reduced to system with three of them. Chosen coordinates are: z_T – vertical position of mass centrum *T*, φ – rotation around lateral axis *y'* (pitch), θ – rotation around longitudinal axis *x'* (roll).

Lagrange equations, second-order partial differential equations are used to describe movement of the modeled platform with integrated weapon [7], induced by the force generated when fired out of it:

$$\frac{\mathrm{d}}{\mathrm{d}t}\left(\frac{\partial E_k}{\partial \dot{q}_i}\right) - \frac{\partial E_k}{\partial q_i} = -\frac{\partial E_p}{\partial q_i} - \frac{\partial \Phi}{\partial \dot{q}_i} + Q'_{q_i} \tag{2}$$

Labeled $i = 1, n$, and n is the number of degrees of freedom for system motion (in this case $n = 3$), E_k – system kinetic energy, E_p – system potential energy, Φ – dissipative function, $\left(-\frac{\partial E_p}{\partial q_i}\right)$ – generalized conservative force (negative partial derivative of potential energy by generalized coordinate *i*), $\left(-\frac{\partial \Phi}{\partial \dot{q}_i}\right)$ – generalized dissipative force (negative partial derivative of dissipative function by generalized velocity *i*), Q'_{q_i} - arbitrary non-conservative generalized force.

Total system kinetic energy consists of mass centrum translator kinetic energy and rotational kinetic energy, around the mass centrum:

$$E_k = \frac{1}{2}\cdot m \cdot \dot{z_T}^2 + \frac{1}{2}\cdot J_y \cdot \dot{\varphi}^2 + \frac{1}{2}\cdot J_x \cdot \dot{\theta}^2 \tag{3}$$

J_y is moment of inertia of system mass in regard to longitudinal axis *y'*, and J_x is moment of inertia of system mass in regard to lateral axis *x'*.

Formula for potential energy of the system, for equal values of spring stiffness coefficients is:

$$E_p = \frac{1}{2}\cdot c_1 \cdot (\Delta_{11}^2 + \Delta_{12}^2) + \frac{1}{2}\cdot c_2 \cdot (\Delta_{21}^2 + \Delta_{22}^2) \tag{4}$$

Labeled Δ_{ij} is total deformation, or displacement of elastic elements. Dissipative function, with calculated derivatives of relative displacements and for equal values of damping coefficients, is

$$\Phi = \frac{1}{2}\cdot k_1 \cdot \left(\dot{\Delta}_{11}^2 + \dot{\Delta}_{12}^2\right) + \frac{1}{2}\cdot k_2 \cdot \left(\dot{\Delta}_{21}^2 + \dot{\Delta}_{22}^2\right) \tag{5}$$

Generalized non-conservative forces are derived using virtual displacement of the point *D* in which actuates external force. For computation maximum value of previously calculated resistance force to recoil R_{max} is used. It has three components in the directions of three axes R_x, R_y и R_z, so the formula for virtual work is:

$$\delta A = (R_x(t) \cdot h + R_z(t) \cdot d) \cdot \delta\varphi + \left(R_y(t) \cdot h\right) \cdot \delta\theta + (-R_z(t)) \cdot \delta z_T \qquad 6)$$

In order to define Lagrange's equations, derivatives of previous formulas for kinetic energy, potential energy, dissipative energy and virtual displacements are appointed and their components sorted by the generalized coordinates. Formed system of differential equations can be noted in matrix form:

$$[A]\{\ddot{q}\} + [B]\{\dot{q}\} + [C]\{q\} = \{Q\} \qquad (7)$$

$[A]$ is matrix of inertia or matrix of masses, $[B]$ is damping matrix, $[C]$ stiffness matrix, and $\{Q\}$ is driving force vector. When substitution of matrixes takes place matrix (7) becomes matrix (8).

$$\begin{bmatrix} m & 0 & 0 \\ 0 & J_y & 0 \\ 0 & 0 & J_x \end{bmatrix} \begin{Bmatrix} \ddot{z_T} \\ \ddot{\varphi} \\ \ddot{\theta} \end{Bmatrix} + \begin{bmatrix} 2 \cdot k_1 + 2 \cdot k_2 & 2 \cdot k_1 \cdot a - 2 \cdot k_2 \cdot b & 0 \\ 2 \cdot k_1 \cdot a - 2 \cdot k_2 \cdot b & 2 \cdot k_1 \cdot a^2 + 2 \cdot k_2 \cdot b^2 & 0 \\ 0 & 0 & 2 \cdot k_1 \cdot s^2 + 2 \cdot k_2 \cdot s^2 \end{bmatrix} \begin{Bmatrix} \dot{z_T} \\ \dot{\varphi} \\ \dot{\theta} \end{Bmatrix} + \begin{bmatrix} 2 \cdot c_1 + 2 \cdot c_2 & 2 \cdot c_1 \cdot a - 2 \cdot c_2 \cdot b & 0 \\ 2 \cdot c_1 \cdot a - 2 \cdot c_2 \cdot b & 2 \cdot c_1 \cdot a^2 + 2 \cdot c_2 \cdot b^2 & 0 \\ 0 & 0 & 2 \cdot c_1 \cdot s^2 + 2 \cdot c_2 \cdot s^2 \end{bmatrix} \begin{Bmatrix} z_T \\ \varphi \\ \theta \end{Bmatrix} = \begin{Bmatrix} -R_z(t) \\ R_x(t) \cdot h + R_z(t) \cdot d \\ R_y(t) \cdot h \end{Bmatrix} \qquad 8)$$

Final matrix (8) is valid for time span [0; 0,0522 s] while resistance force to recoil impacts the system and while oscillations of the platform with integrated weapon have driven-damped character.

After excitation ceases, the system continues to oscillate damped by the absorbers until it stops in equilibrium position. Matrix that describes free damped oscillating motion of the wheeled platform with integrated weapon and three degrees of freedom:

$$\begin{bmatrix} m & 0 & 0 \\ 0 & J_y & 0 \\ 0 & 0 & J_x \end{bmatrix} \begin{Bmatrix} \ddot{z_T} \\ \ddot{\varphi} \\ \ddot{\theta} \end{Bmatrix} + \begin{bmatrix} 2 \cdot k_1 + 2 \cdot k_2 & 2 \cdot k_1 \cdot a - 2 \cdot k_2 \cdot b & 0 \\ 2 \cdot k_1 \cdot a - 2 \cdot k_2 \cdot b & 2 \cdot k_1 \cdot a^2 + 2 \cdot k_2 \cdot b^2 & 0 \\ 0 & 0 & 2 \cdot k_1 \cdot s^2 + 2 \cdot k_2 \cdot s^2 \end{bmatrix} \begin{Bmatrix} \dot{z_T} \\ \dot{\varphi} \\ \dot{\theta} \end{Bmatrix} + \begin{bmatrix} 2 \cdot c_1 + 2 \cdot c_2 & 2 \cdot c_1 \cdot a - 2 \cdot c_2 \cdot b & 0 \\ 2 \cdot c_1 \cdot a - 2 \cdot c_2 \cdot b & 2 \cdot c_1 \cdot a^2 + 2 \cdot c_2 \cdot b^2 & 0 \\ 0 & 0 & 2 \cdot c_1 \cdot s^2 + 2 \cdot c_2 \cdot s^2 \end{bmatrix} \begin{Bmatrix} z_T \\ \varphi \\ \theta \end{Bmatrix} = \begin{Bmatrix} 0 \\ 0 \\ 0 \end{Bmatrix} \qquad (8)$$

Differential equations are solved for the data defined in advance: firing conditions (elevation angle, azimuth angle, pressure force in the barrel and resistance force to recoil) and vehicle/platform construction parameters (stiffness and damping coefficients, mass centrum coordinates and moments of inertia). This way, platform oscillation equations are obtained, and for them, in regard to time, change of the generalized coordinates and velocities of those changes.

5. SIMULATION OF MOBILE PLATFORM OSCILLATIONS AND RESULTS ANALYSIS

Solving of previously defined system of differential equations represents the main part of the simulation and it was conducted numerically in MATLAB environment. There are three initial data sets: vehicle data – technical data, vehicle mass centrum position, vehicle elastic suspension characteristics, moments of inertia; weapon data – weapon mass, integrating position relative to system mass centrum, elevation and azimuth angles; driven force data – calculated values of resistance force R over time.

For integration point, position on the rooftop above back seat was selected. In Table 2 are shown values of these data for basic setup of the system, used for computation. Labels d and h are horizontal and vertical distances of weapon integration position from mass centrum of vehicle-weapon system, respectively.

Table 2. Weapon data and its basic position

AGL 30 mm M93	
Weapon mass with ammunition, m_o [kg]	38
Horizontal distance of the weapon from the mass centrum, d [m]	0,929
Vertical distance of the weapon from the mass centrum, h [m]	1,033
Elevation angle, α [°]	30
Azimuth angle, β [°]	45

Code in MATLAB uses these data to calculate system mass centrum and solve defined matrixes so generalized coordinates over time are determined – translation of mass centrum and angular displacements, as well as their graphical representation. For analysis purposes of recoil process on platform oscillations when firing integrated weapon, elevation and azimuth angles are varied, and so is the weapon position on the vehicle.

Selected angle values for calculations include boundary conditions for firing automatic grenade launcher mounted on vehicle of choice and an angle between them. Elevation angles are $\alpha = [0°, 30°, 60°]$ and azimuth angles are $\beta = [0°, 45°, 90°]$. For different combination of these angles changes of generalized coordinates are acquired. Label $z_T(t)$ represents translation of system mass centrum relative to basic position over time; $\varphi(t)$ is angular displacement of the system around its mass centrum in *xz* plane over time, relative to basic position, so called pitch and $\theta(t)$ is angular displacement of the system around its mass centrum in *yz* plane over time, relative to basic position, so called roll. Initial values of the generalized coordinates are $z_T(0) = 0$ m; $\varphi(0) = 0°$; $\theta(0) = 0°$.

Vital parameters are segregated out of the results and shown in Table 3 for better review and comparison. Segregated parameters are generalized coordinates amplitudes, time needed to reach amplitude (t_A) and time required for system to stops in equilibrium position (t_S).

Table 3. Computation results of system oscillations for different elevation and azimuth angles

α	**β**	Coordinates	Amplitude	t_A [s]	t_S [s]
0°	0°	z_T [mm]	-0,08	0,36	1,5
		φ [mrad]	5,86	0,31	1,26
		θ [mrad]	0	0	0
	45°	z_T [mm]	-0,056	0,36	1,4
		φ [mrad]	4,14	0,31	1,35
		θ [mrad]	14,61	0,31	1,35
	90°	z_T [mm]	0	0	0
		φ [mrad]	0	0	0
		θ [mrad]	20,66	0,31	1,35
30°	0°	z_T [mm]	-6	0,35	1,82
		φ [mrad]	5,11	0,31	1,35
		θ [mrad]	0	0	0
	45°	z_T [mm]	-4,26	0,35	1,72
		φ [mrad]	3,61	0,32	1,28
		θ [mrad]	12,65	0,32	1,28
	90°	z_T [mm]	0	0	0
		φ [mrad]	0	0	0
		θ [mrad]	17,89	0,32	1,25
60°	0°	z_T [mm]	-10,37	0,35	1,95
		φ [mrad]	2,99	0,31	1,25
		θ [mrad]	0	0	0
	45°	z_T [mm]	-7,33	0,36	1,65
		φ [mrad]	2,12	0,31	1,25
		θ [mrad]	7,31	0,31	1,25
	90°	z_T [mm]	0	0	0
		φ [mrad]	0	0	0
		θ [mrad]	10,33	0,31	1,25

With an increase of the azimuth angle, for constant elevation angle, angular displacement θ (roll) is increasing, while angular displacement φ (pitch) and mass centrum translation z_T are decreasing. Approximately the same amount of time is required for generalized coordinates to reach their amplitude. Time required for system to stop in equilibrium position is longest for the translator displacement z_T.

Value of the vertical translation z_T and angular displacement in *xz* plane φ notably impacts weapon precision, that is, it can cause shot deviation on target. Data in Table 3 show that amplitudes of those displacements are significant. Rate of fire is tightly dependent on time needed for system to stop in equilibrium position, because every deviation from basic firing position will not give satisfying results. Now it can be concluded that for this type of integration AGL onto the vehicle, it is better to use lower rate of fire or single fire. Angular displacement in *yz* plane θ creates rotated shooting plane, but does not affect precision. It should be noted that these values are larger than the real ones, because maximum value of the force transferred to the platform was used.

Besides the varying of the elevation and azimuth angles, position of the weapon on the vehicle is also altered (Table 4). For further computation, medium values of these angles were selected ($\alpha = 30°$ and $\beta = 45°$). For horizontal (d) and vertical (h) distance of the weapon integration point from the point T chosen values are $d =$ [0,929 m; 2,787 m; -1,393 m] and $h =$ [1,033 m; 0,619 m; 0,103 m]. While varying horizontal distance, vertical distance keeps main value, and vice versa (given in Table 2). Figure 7 is graphical representation of system oscillations for different sets of weapon position coordinates on the platform.

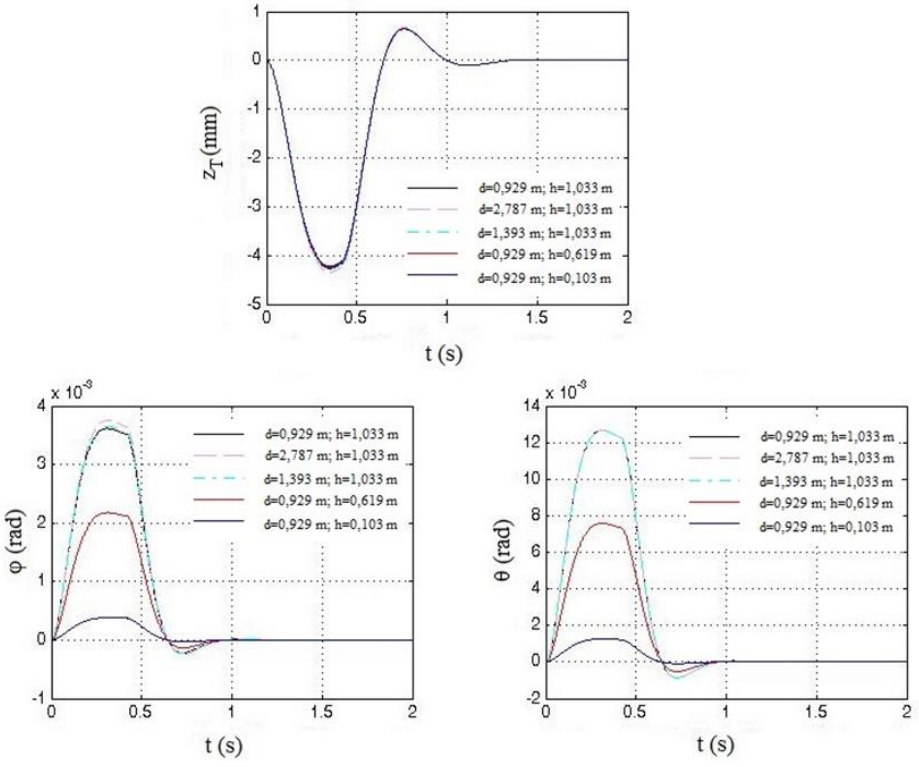

Figure 7. Change of generalized coordinates z_T, φ, θ over time for several weapon positions

These results are displayed in Table 4 in numerical form.

Table 4. Computation results of system oscillations for different position of the weapon on the platform

Distance	Coordinates	Amplitude	t_A[s]	t_S[s]
d = 2,787 m	z_T [mm]	-4,34	0,35	1,62
	φ [mrad]	3,75	0,31	1,3
	θ [mrad]	12,65	0,32	1,28
d = -1,393 m	z_T [mm]	-4,18	0,35	1,62
	φ [mrad]	3,45	0,29	1,12
	θ [mrad]	12,65	0,32	1,21
h = 0,619 m (H_T = 1010,9 m)	z_T [mm]	-4,24	0,35	1,71
	φ [mrad]	2,18	0,31	1,09
	θ [mrad]	7,58	0,31	1,21
h = 0,103 m (H_T = 1001,8 m)	z_T [mm]	-4,22	0,35	1,85
	φ [mrad]	0,38	0,32	1,11
	θ [mrad]	1,26	0,32	1,21

Moving the weapon integration position toward the back or the front part of the vehicle, amplitudes of the chosen parameters practically do not change. Alterations made to weapon position in vertical direction have more influence on generalized coordinates then changes in horizontal direction. When the integration point is closer to the mass centrum, amplitude of the angular displacement θ significantly decreases, amplitude of the angular displacement φ decreases, as well as the time required for the system to stop in equilibrium position (for angular displacements).

6. CONCLUSIONS

Studied in this paper is simplified platform-armament model in order to analyze impact of firing process on light mobile wheeled platform oscillations. Automatic grenade launcher 30 mm M93 is mounted on the Land Rover Defender's rooftop and the goal is that suspension handle additional loads generated when firing weapon, absorbs them adequately so precision on target is maintained. Low precision occurs as a consequence of unsuitable system oscillation evoked by force that transfers to the platform. This paper only pertains recoil process during one fired shot and its impact on system oscillations.

Defined simplified model has three degrees of freedom, mass centrum translation in vertical z axis direction and rotations around longitudinal x axis and lateral y axis. Vertical, longitudinal and lateral system dynamics is studied in two planes, which includes motions vital for oscillation analysis. As a result, generalized coordinates over time are created.

Vertical translation z_T changes as much as 10 mm for high elevation angles. Angular displacement φ has the greatest impact on precision and goes over 5 mrad for zero elevation and azimuth angles, which causes projectile to miss target by 5 meters on 1000 meters distance. Angular displacement θ has the biggest value for zero elevation and maximum azimuth angle, but only rotates shooting plane, precision is not effected. Alterations made to weapon position in vertical direction have more influence on generalized coordinates then changes in horizontal direction. For weapon position close to the mass centrum vertical translation z_T practically does not change, but angular displacements decrease, θ far more then φ. For a precise hit, at 1000 meters distances, displacement of $\varphi = 2 \div 3$ mrad is too much. As mentioned in paper, it shoud be taken into account that those are oversized values, obtained when maximum recoil force was used. More extensive varying of weapon position

on the platform would enable defining optimal integration point in order to achieve higher rates of fire, preferably maximal rate.

Outcome accuracy depends on quality of the real system simplification. If experimental results are available comparison with the theoretical model can be conducted and simplified model assessed. At last, practical tests can give insight how theoretical model could be updated and, in that way, made more realistic.

First step toward more realistic model is to use variable force transferred to the platform over time, not only its maximum value, and to include process of the recoil mass restoring to starting position in the computation, as well. Extension of the paper can be creating more complex mathematical model with more degrees of freedom and separated masses of integrated components. Elastic suspension system could have more complex geometry or some existing configuration could be acquired. Also, stiffness and damping coefficients could be altered and their impact on the system oscillations monitored. With some adjustments, upgraded model could be used for other weapons and platforms.

REFERENCES

[1] Jaramaz. S., Micković D. Primena principa komore visokog/niskog pritiska na optimizaciju pogona municije za automatski bacač granata, Mašinski fakultet, Beograd, 2001.

[2] Uputstvo za korišćenje i održavanje – 30 mm bacač granata automatski, Zastava oružje.

[3] Cvetković M. Unutrašnja balistika, Vojnoizdavački zavod, Beograd, 1998.

[4] Petrović M. Mehanika automatskog oružja, Vojnoizdavački zavod, Beograd, 2009.

[5] Petrović M. Mehanika automatskog oružja, Vojnoizdavački zavod, Beograd, 2009.

[6] Simić D. Motorna vozila, treće izdanje, IRO „Naučna knjiga“, Beograd, 1988.

[7] Rašković D. Teorija oscilacija, treće izdanje, Građevinska knjiga, Beograd 1974.

MVM – International Journal for Vehicle Mechanics, Engines and Transportation Systems

NOTIFICATION TO AUTHORS

The Journal MVM publishes original papers which have not been previously published in other journals. This is responsibility of the author. The authors agree that the copyright for their article is transferred to the publisher when the article is accepted for publication.

The language of the Journal is English.

Journal ***Mobility & Vehicles Mechanics*** is at the SSCI list.

All submitted manuscripts will be reviewed. Entire correspondence will be performed with the first-named author.

Authors will be notified of acceptance of their manuscripts, if their manuscripts are adopted.

INSTRUCTIONS TO AUTHORS AS REGARDS THE TECHNICAL ARRANGEMENTS OF MANUSCRIPTS:

Abstract is a separate Word document, "*First author family name_ABSTRACT.doc*". Native authors should write the abstract in both languages (Serbian and English). The abstracts of foreign authors will be translated in Serbian.

This document should include the following: 1) author's name, affiliation and title, the first named author's address and e-mail – for correspondence, 2) working title of the paper, 3) abstract containing no more then 100 words, 4) abstract containing no more than 5 key words.

The manuscript is the separate file, „*First author family name_Paper.doc*" which includes appendices and figures involved within the text. At the end of the paper, a reference list and eventual acknowledgements should be given. References to published literature should be quoted in the text brackets and grouped together at the end of the paper in numerical order.

Paper size: Max 16 pages of B5 format, excluding abstract
Text processor: Microsoft Word
Margins: left/right: mirror margin, inside: 2.5 cm, outside: 2 cm, top: 2.5 cm, bottom: 2 cm
Font: Times New Roman, 10 pt
Paper title: Uppercase, bold, 11 pt
Chapter title: Uppercase, bold, 10 pt
Subchapter title: Lowercase, bold, 10 pt
Table and chart width: max 125 mm
Figure and table title: Figure _ (Table _): Times New Roman, italic 10 pt

Manuscript submission: application should be sent to the following e-mail:

mvm@kg.ac.rs ; lukicj@kg.ac.rs
or posted to address of the Journal:
University of Kragujevac – Faculty of Engineering
International Journal M V M
Sestre Janjić 6, 34000 Kragujevac, Serbia

The Journal editorial board will send to the first-named author a copy of the Journal offprint.

MVM – International Journal for Vehicle Mechanics, Engines and Transportation Systems

OBAVEŠTENJE AUTORIMA

Časopis MVM objavljuje orginalne radove koji nisu prethodno objavljivani u drugim časopisima, što je odgovornost autora. Za rad koji je prihvaćen za štampu, prava umnožavanja pripadaju izdavaču.

Časopis se izdaje na engleskom jeziku.

Časopis ***Mobility & Vehicles Mechanics*** se nalazi na SSCI listi.

Svi prispeli radovi se recenziraju. Sva komunikacija se obavlja sa prvim autorom.

UPUTSTVO AUTORIMA ZA TEHNIČKU PRIPREMU RADOVA

Rezime je poseban Word dokument, "*First author family name_ABSTRACT.doc*". Za domaće autore je dvojezičan (srpski i engleski). Inostranim autorima rezime se prevodi na srpski jezik. Ovaj dokument treba da sadrži: 1) ime autora, zanimanje i zvanje, adresu prvog autora preko koje se obavlja sva potrebna korespondencija; 2) naslov rada; 3) kratak sažetak, do 100 reči, 4) do 5 ključnih reči.

Rad je poseban fajl, „*First author family name_Paper.doc*" koji sadrži priloge i slike uključene u tekst. Na kraju rada nalazi se spisak literature i eventualno zahvalnost. Numeraciju korišćenih referenci treba navesti u srednjim zagradama i grupisati ih na kraju rada po rastućem redosledu.

Dužina rada: Najviše 16 stranica B5 formata, ne uključujući rezime
Tekst procesor: Microsoft Word
Margine: levo/desno: mirror margine; unurašnja: 2.5 cm; spoljna: 2 cm, gore: 2.5 cm, dole: 2 cm
Font: Times New Roman, 10 pt
Naslov rada: Velika slova, bold, 11 pt
Naslov poglavlja: Velika slova, bold, 10 pt
Naslov potpoglavlja: Mala slova, bold, 10 pt
Širina tabela,dijagrama: max 125 mm
Nazivi slika, tabela: Figure __ (Table _): Times New Roman, italic 10 pt

Dostavljanje rada elektronski na E-mail: **mvm@kg.ac.rs ; lukicj@kg.ac.rs**

ili poštom na adresu Časopisa
Redakcija časopisa M V M
Fakultet inženjerskih nauka
Sestre Janjić 6, 34000 Kragujevac, Srbija

Po objavljivanju rada, Redakcija časopisa šalje prvom autoru jedan primerak časopisa.

MVM *Editorial Board*
University of Kragujevac
Faculty of Engineering
Sestre Janjić 6, 34000 Kragujevac, Serbia
Tel.: +381/34/335990; Fax: + 381/34/333192
www.mvm.fink.rs